Bachelor Thesis

Safety module

for a High Frequency Arbitrary Waveform Neural Stimulator

F. Varkevisser & L.A. Enthoven

REValUE Project

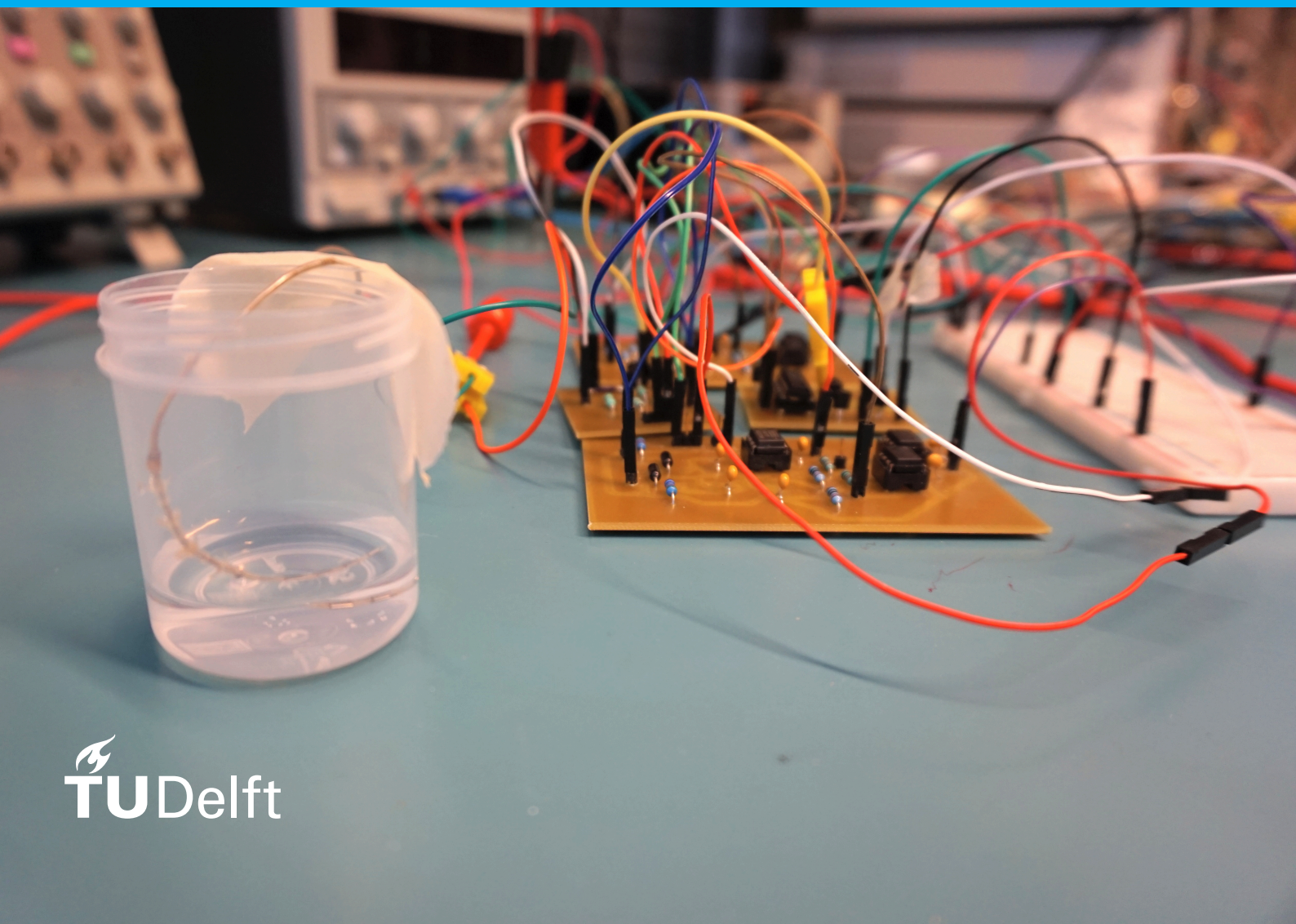

TU Delft

Bachelor Thesis

Safety Module for a High Frequency Arbitrary Waveform Neural Stimulator

by

F. Varkevisser & L.A. Enthoven

to obtain the degree of Bachelor of Science
at the Delft University of Technology,
to be defended on Friday June 22, 2018

Student numbers:	4362233, 4358678	
Project duration:	April 23, 2018 – June 22, 2018	
Thesis committee:	Dr. ing. I.E. Lager,	Associate Professor Terahertz Sensing (THZ), Department of Microelectronics, TU Delft, Chair
	Prof. dr. ir. W.A. Serdijn,	Chairman Bioelectronics (BE), Department of Microelectronics, TU Delft, supervisor
	Dr. B.F.M. Blok,	Urologist and Head of the Department of Urology, Erasmus Medical Center, client supervisor
	Dr. S. Izadkhast,	Principal Electrical Engineering (EE) Educator at the EE Education (EEE) group within the Microelectronics (ME) department.

TU Delft

Abstract

The goal of the REValUE Project is to design a test device which is able to stimulate nerve tissue with current driven, high frequency stimulation in the range from 1 to 15 kHz and 1 to 10 mA. The test device will be used in research to pudendal nerve blockage.

This thesis describes the design process of a safety module for this device. The safety module should guarantee that every stimulation with the device is within the safe stimulation parameters, it should stop any stimulation signal that exceeds 15 mA, 10.5 V or 30 $\mu C/cm^2$. In this thesis a design is proposed that can detect over stimulation. In case of over stimulation, further stimulation is stopped and the stimulated tissue is discharged. Additionally, the module discharges the tissue when the device is shut off.

The prototype built during this project is able to stop signals that exceeds 26.7 $\mu C/cm^2$, 15.5 mA and 11 V. Design adjustments to improve the performance of the device are proposed in the discussion section, after which the module will be able to prevent exceeding the safety parameters. The requirement for DC blockage turned out to be an issue in the proposed design. An alternative topology has been thought of, but because of time limits the new design could not be tested. After the improvements proposed in chapter 10, the system should meet all the requirements and guarantee safe stimulation.

Preface

This thesis has been made in cooperation with Max Engelen, Philip van den Heuvel, Simon Verkleij and Tom Salden. A big thanks to them for being our project partners and for their help and support during this project. We want to thank our thesis supervisor Wouter Serdijn, for bringing us good feedback and brainstorming with our ideas. Bertil Blok for the interesting project and the active feedback we have gotten. Ali Kaichouhi for the techincal support and help with PCB's. Marion de Vlieger for helping us coordinate everything properly. Additional thanks to Jan Groen, Gerard Baquer and Willem van 't Leven, who have all helped this thesis become what it is now.
Furthermore we want to thank our family and friends for the support they have given us throughout this period.

Francesc Varkevisser & Luc Enthoven
Delft, June 2018

Contents

1 Introduction

This project is done in cooperation with two other groups [1, 2], all groups concern the same problem but work on different sub modules for this project. Therefore, the project introduction, problem definition and project objective found in the theses are the same.

1.1. Introduction to the REValUE Project

Millions of people have difficulty in emptying their urinary bladder [3]. Well-known causes are *spinal-cord injury* (SCI) and *multiple sclerosis* (MS), but many more non-neurological patients suffer from similar problems without an obvious cause. Normally, the urethral sphincter is continuously contracted and only a few times per day relaxed during voiding. This relaxation is controlled by a switch in the brainstem [4]. When the brainstem switch is not activated, there is no relaxation of the sphincter and, thus, no voiding and the sphincter remains contracted and closed. Patients in retention cannot void because they are unable to activate the brainstem switch.

1.1.1. Problem Definition

The most common treatment is to mechanically empty the bladder with intermittent self catheterization or an indwelling catheter as there is no treatment to restore the voiding function [5]. Using a catheter results in infections, pain and excessive healthcare costs [6]. Electrical stimulation to improve bladder function has been utilized with varying success [7]. The Bindley system has been implanted which uses sacral root stimulation where the roots are selectively cut. This method is irreversible and causes total absence of erections. The rhizotomy and implantation take more than five hours of surgery and both urologists and neurosurgeons are necessary for the operation.
Sacral nerve stimulation is an often used technique for bladder voiding in patients without SCI [8]. This method only needs percutaneous access to the nerves, significant reducing the surgery time. The downside of this method is that the urethra is still closed, resulting in a high bladder pressure and an increased chance that urine flows back into the kidneys.

1.1.2. Project Objective

In this project, a high frequency stimulator is developed. The high frequency signal cancels the blocking of the urethral sphincter. A study has shown effective emptying of the bladder of cats by blocking the pudendal nerves [9]. Besides high frequency stimulation, the project is aimed to develop a low frequency stimulator as well, to stimulate the ventral roots, causing bladder contraction.
For this goal, a Bachelor Graduation Project group from Electrical Engineering was formed. The objective of this group was to develop a high frequency, arbitrary-waveform, neural stimulation device that offers efficacious, yet safe, stimulation of the pudendal nerves. This can be used to focus on relaxing the urethral sphincter by reversible, bilateral, high frequency blocking of the pudendal nerves to enable voiding. After emptying the urinary bladder, the

blockage is stopped and the sphincter resumes its normal closure function during continence.
This group of six people is divided in teams of two. The first team focuses on the interface and the control of the device. The second team develops the waveform generator circuit and a third team makes the safety system of the waveform generator.

1.1.3. State-of-the-art Arbitrary Waveform Neural Stimulator Analysis

The state of the art neural stimulators are integrated circuits because they have restrictions on the power and the size of the device. Most arbitrary waveform generators are however made with discrete components [10]. Furthermore, most state-of-the-art neural stimulators have been made for testing and implementation on small animals and not for humans [10, 11]. When there are no power and size limitations the arbitrary waveform generators are often implemented using a current controlled stimulation [10].
Most state-of-the-art stimulators are based on low frequency stimulation (1-100 Hz). Low frequency stimulation can produce neural response, while high frequency stimulation results the blockage of these neural responses [12]. High frequency stimulators do exist for other applications than pudendal nerve stimulation, which this project is focussed on [13]. The stimulator designed in this project will stimulate at both high and low frequency, which does not exist currently.
At the start of the research, the Medtronic 3625 Test Stimulator has been used for arbitrary low frequency bladder stimulation in the hospital. The Test Stimulator is a voltage controlled device and has the following characteristics: amplitude range 0-10 V with a $\pm$0.5 V accuracy and a variable pulse width between 50-1000 μs [14].

1.2. Safety Considerations in Stimulation of the Human Body

As this report covers the safety aspect of the neural stimulators, it is important to have knowledge about what is considered safe in the human body and what causes damage to the human body. Research was done to the effects of different types of stimulation and what amplitudes must not be exceeded to ensure safe stimulation.

1.2.1. Effects of Tissue Stimulation in the Human Body

When stimulating in the human body, charge is injected. This charge can cause two types of chemical reactions in the body: non-Faradaic reactions and Faradaic reactions [15]. In Non-Faradaic reactions, charge in the tissue is redistributed due to charge injection whereas with Faradaic reactions, electrons react with chemicals in the human body. Some Faradaic reactions are reversible, others are not. Additionally, dependent on the type of stimulation, either by adding electrons to the body or by removing electrons from the body, different Faradaic reactions are caused. Too much charge on the electrode tissue interface could cause irreversible chemical reactions, which can cause serious damage to the tissue [15].

1.2.2. Currently Used Stimulation Types

There are multiple ways to stimulate the tissue, this can be done via either monophasic or biphasic pulses. For these type of pulses, cathodic (negative current into the tissue, charge is added) and anodic (positive current into the tissue, charge is removed) phases are defined [11]. Monophasic stimulation only consists of stimulation with a cathodic phase, whereas biphasic stimulation uses both a cathodic and anodic phase to stimulate the tissue. A study has shown that high frequency monophasic stimulation causes more damage to brain tissue than biphasic stimulation [16]. Monophasic stimulation can safely be used if the stimulation frequency is low and the tissue can be shortened between the cathodic phases to prevent charge build-up at the tissue. Biphasic stimulation can be used both with low and high frequency and has been proven to be safe when the stimulation parameters are within safe limits [16–18].

1.2.3. Safe Stimulation Parameters

It is important to derive safe stimulation parameters independent of what is specified by the other subgroups of this project [1, 2]. The safe stimulation parameters have been established by looking at different stimulation devices that are currently on the market and by doing literature study. It has been found that assuming a tissue impedance of 500 Ω, a maximum current of 15 mA can be used [19, 20]. The maximum voltage that can be put over the tissue has been found to be 10.5 V [14, 21]. The maximum charge density per phase is found to be 30 μ C/cm^2/phase [14], it is important to note that the surface roughness of the electrode can increase the stimulation area of the electrode [22].
Since the parameters listed above are used in devices for long term stimulation, it is considered that these parameters are safe enough for the short duration stimulation of the to be designed device. Therefore, long term effects of stimulation with these parameters will not be considered at this moment.

1.2.4. Direct Current Blockage in the Stimulation Signal

Direct Currents (DC) through the tissue can cause serious damage [23, 24]. Therefore it should be assured that any DC offset in the stimulation signal is filtered out in order to have safe stimulation. During research it was found that almost every neural stimulation device on the market uses capacitive coupling to achieve this [23, 25].

1.2.5. Single Fault Safety Condition

The protection from a single fault condition is implemented in most of the design steps of medical equipment [26]. One important aspect when making a hardware design is the safe shut-down of the system in case of an error. In this report, it is assumed that the fault will be detected by the user of the device, who will shut off the system at that point.

1.3. Thesis Outline

After this introduction, a list of requirements for the safety module is presented in chapter 2. In chapter 3, a brief overview of the full neural stimulator and the place of the safety module in this design is given. Then, a more in depth system level overview of both the safety module and the complete system is given. Chapters 4, 5, 6, 7 and 8 discuss for each sub module of the safety module the process of design, implementation and prototyping. After testing each sub module on proper functioning, measurements on the combined module are presented in chapter 9. The resulting module is discussed in chapter 10. Finally chapter 11 concludes the thesis and proposes future research.

2

Program of Requirements

As described in the introduction, the goal of the REValUE project is to deliver a neural stimulator which can be used to determine optimal parameters for urinary bladder stimulation. In order to deliver such a system, a program of requirements was determined. Because the project consists of different subgroups, a list of general requirements was formulated to clarify the demands of the client which every subgroup needs to consider. For the design of a safety module for this system, a list of specific safety requirements was formulated. The general and safety requirements are presented in this chapter.

2.1. General Requirements of the Project

The general requirements of the total system will not be further discussed in this report during the design steps, they are however always kept in mind during the design process. The following general requirements are set for the project [1, 2]:

- The device should have 2 identical connections for 2 extension cables which are connected to a lead. The lead has an array with 4 electrodes (Lead used is Medtronic Model 388928).
- The leads must be connected with an extension cable which should fit the connectors of the device.
- The device must be able to stimulate on all possible terminals of the lead.
- The device must support monopolar and bipolar stimulation.
- The device must operate outside the sterile field around the patient.
- The device must not cost more than €5,000.
- The device must not be larger than $0.5 \times 0.5 \times 0.3$ meters (length x width x height).
- The device must not weigh more than 10 kg.
- The components of the device must ensure a lifetime of at least 6 months.
- The device must be able to operate between 10° and 40° C.
- The internal temperature of the device must be kept in a range where the device is still fully functioning (so where the device meets all specified requirements).
- The device must not create sounds which exceed 40 dB [27].
- The device must be made from commercial off-the-shelf components.

Requirements to apply injected charge

Primary Requirement

The generated waveform must be current driven. The device must independently control the current through two (implantable) leads with both four electrodes. The current through all electrodes must be controlled independently in two different channels.

Secondary Requirement
Besides a current driven waveform, the device must be able to generate a voltage driven waveform.

2.2. Program of Requirements Safety Subgroup

2.2.1. Functional Requirements of the Safety Module

The safety module will monitor the charge, current and voltage that will be the output of the waveform module. The module has to guarantee safe stimulation. If other modules lose power or cause dangerous stimulation, the safety module should independently guarantee the fault safety to ensure the safety of the patient.

Input of Safety Module
The input signal of the safety module is the waveform generated for stimulation.

Output of Safety Module
The output signal of the safety module is an electrode switch which can switch between any of the 4 electrodes of the lead. For bilateral, stimulation two safety modules will be used in parallel which will be connected to two electrode switches.

Signal Transfer
When the maximum charge, current or voltage, as specified in the system requirements, are not exceeded, the safety module must pass the stimulation waveform to the output. When one of the measured quantities exceeds the requirements, the signal must be interrupted. DC components of the provided signal must be blocked.

2.2.2. System Requirements of the Safety Module

Single Fault Safety
When shutting down, the safety module should always guarantee to fully discharge the tissue.

Injected Charge
The injected charge to the tissue is the primary measured quantity of the module, charges above 30 $\mu C/cm^2$ at the surface of the electrodes must be prevented [14].

Injected Current
The safety module must prevent currents above 15 mA to be injected into the tissue [19, 20].

Induced Voltages
The safety module must prevent voltages above 10.5 V to be put over the tissue [14].

3

Module Overview

In the introduction, the design of an arbitrary waveform neural stimulator for high frequencies has been proposed. This chapter presents the division of work and the interpretation of the program of requirements, given in chapter 2, to sub modules. A system level overview of the neural stimulator can be seen in Figure 3.1. The safety module is discussed in section 3.1 and a detailed overview of the entire system is given in section 3.2

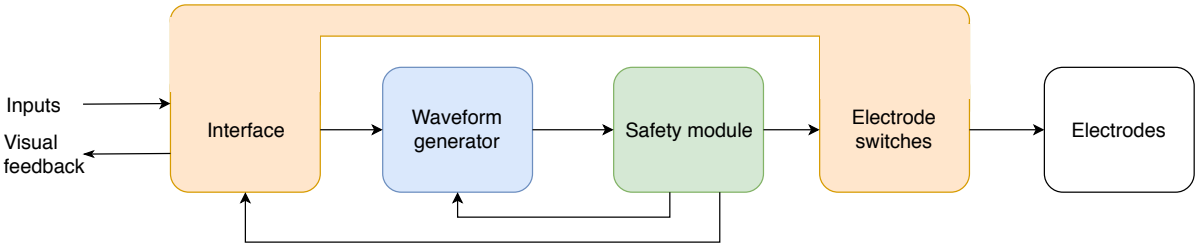

Figure 3.1: System level overview of complete stimulator. The orange blocks are implemented by the interface subgroup [1], the blue block is implemented by the waveform subgroup [2] and the green blocks are discussed in this report. The white block is not discussed in this project.

3.1. Safety Sub Modules

In order to fulfil the requirements for the safety module given in chapter 2, the following sub modules have to be implemented: A current detector, a voltage detector, a charge integrator, a single fault safety switch and a coupling capacitor. A system level overview of the module can be seen in Figure 3.2.
The current detector, voltage detector and charge integrator will prevent wrong stimulation parameters. These sub modules give a signal to the *error signal combiner* sub module in case of faulty stimulation, which will stop the stimulation and ground the electrode allowing it to discharge. The coupling capacitor prevents DC currents to be injected into the tissue. The single fault safety switch guarantees the single fault safety condition.
The voltage detector is put after the coupling capacitor in order to measure the voltage over the tissue without a DC offset. The single fault safety switch is also put after the coupling capacitor, this way the tissue is discharged as much as possible when the power of the system is off. Since the charge integrator filters out a big part of the input signal, a copy of the stimulation current is required for this sub module.
The electrode switches are implemented by the interface subgroup [1]. These switches are visible on the interface and this prevents multiple copies of the safety sub modules to be needed.

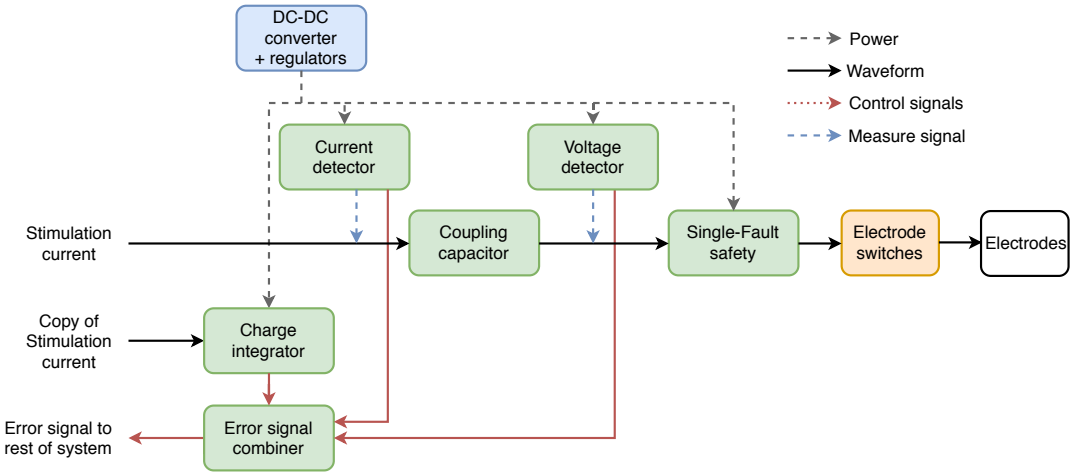

Figure 3.2: Block diagram of safety module. The green blocks are discussed in this report. The blue block is implemented by the waveform subgroup [2] and the orange block is implemented by the interface subgroup [1]. The white block is not discussed in this project.

3.2. Complete System

Figure 3.3 shows the complete neural stimulator in detail. There are two current signals coming from the H-Bridge, these signals are floating between two nodes and are thus not grouded [2]. For the powering of the system, it was chosen to use +15 V single-supply voltage, this should be kept in mind during the design process. The system works from a 9 V battery, the DC-DC converters and regulators are used to provide the right supply voltages for each system.

The colours of the blocks show which group has the responsibility for each sub module. The design of all the orange blocks can be found in the interface report [1], the design of the blue blocks can be found in the waveform report [2] and the design of the green blocks will be discussed in this report.

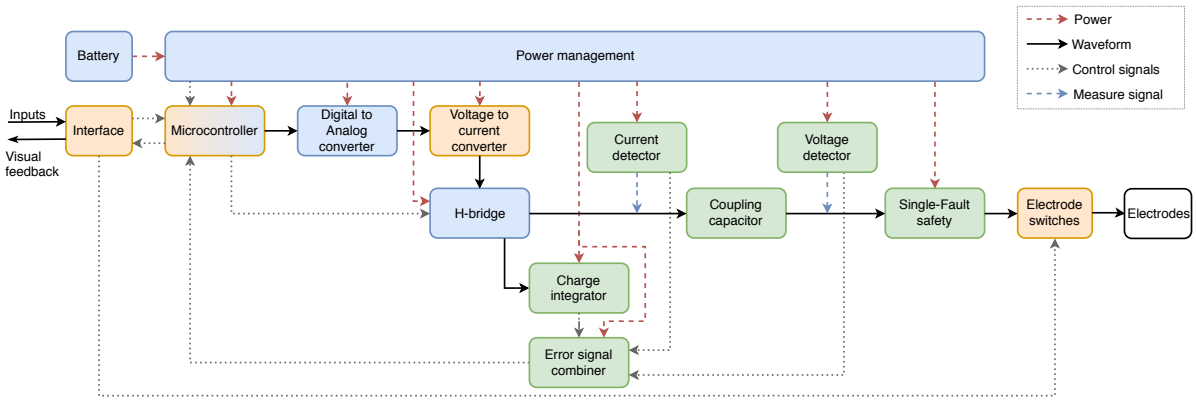

Figure 3.3: Block diagram of the complete stimulator. The green blocks are discussed in this report. The blue blocks are implemented by the waveform subgroup [2] and the orange blocks are implemented by the interface subgroup [1]. The white block is not discussed in this project.

4

Detectors

In order to prevent overcurrent and overvoltage, a current and a voltage detector have been implemented. Because the sub modules resulted in similar topologies, both detectors are discussed in this chapter where similarities and differences will be emphasised. In the design section the design process of the voltage detector will be discussed and a explanation why this design can be used for current detection as well is given. In the implementation section the component choices for both the detectors will be explained. Finally, the prototype section will discuss both prototypes separately.

4.1. Design of the Detector Sub Modules

4.1.1. Design of the Overvoltage Detector

To avoid potentials greater than 10.5 V to be put over to the tissue, the overvoltage detector had to be designed. The detector must monitor the potential over the tissue and trigger the error module in case of over voltage.
The designed circuit for the detector can be seen in Figure 4.1.
The detector follows the voltages at both electrodes. To minimise the current drawn by the detector from the stimulation signal, the input is buffered by two voltage followers. The high input impedance of the buffers will draw very low currents and the current needed for the rest of the detector module is provided by the input buffers. The input voltage for these buffers is divided by resistive voltage dividers with high resistor values for two reasons. Firstly, the needed power supply for the buffers decreases since the output signal of a buffer is often limited by the supply voltage. Secondly, it protects the tissue from high DC currents in case of device failure. In the breakdown case where the supply voltage is put on the input signal, the resistors will limit the current that can flow into the tissue which is certainly important since the voltage detector is operating after the coupling capacitor.
The difference of the output signals of both input buffers is amplified with a factor 1 by a differential amplifier. The differential amplifier rejects the common mode voltage between both signals, which means that it only amplifies the difference of the voltages. The output signal of the differential amplifier is compared by two comparators with a reference voltage to detect positive or negative overvoltage. In order to use the same reference voltage for both comparators, the input signal for the negative comparator is inverted by an inverting voltage amplifier with unity amplification.

4.1.2. Design of the Overcurrent Detector

The circuit for overvoltage detection can also be used for overcurrent detection. Since the stimulation of the tissue is current driven, a resistive load in series with the tissue will not influence charge that is put into the tissue. Thus for the overcurrent detector, a resistor R_{sensor} with a known, accurate value will be put in series with the tissue. The current detector measures the voltage at both terminals of R_{sensor}. The input of the circuit can be seen in Figure 4.2

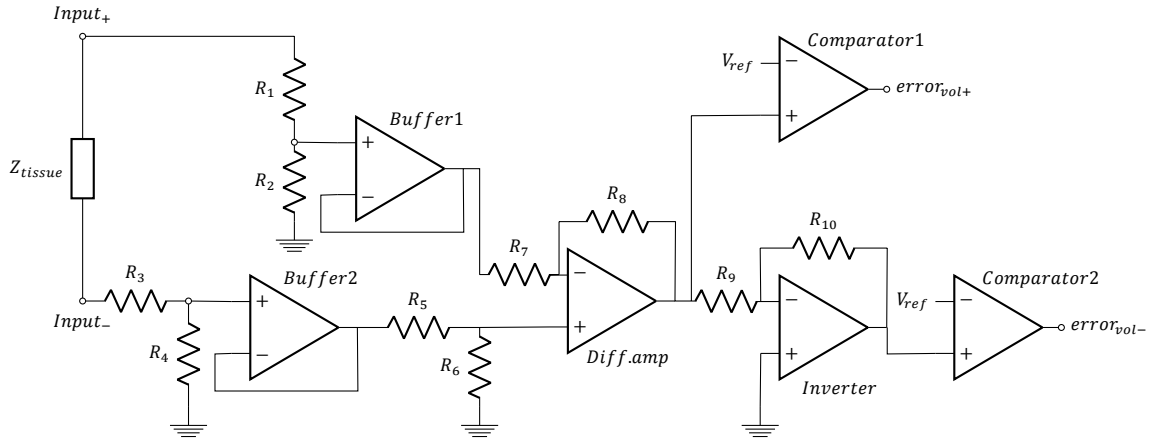

Figure 4.1: Overvoltage detector topology.

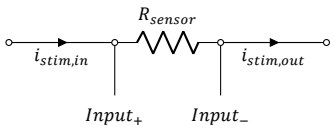

Figure 4.2: Overcurrent detector input topology.

4.2. Implementation of the Detector Sub Modules

In this section the implementation of the current detector will be discussed. Then the differences in the implementation of the voltage detector will be elaborated. Finally, simulations of both circuits will be presented.

4.2.1. Implementation of the Overcurrent Detector

R_{sensor}

The first consideration made for the current detector implementation, as presented in subsection 4.1.2, was the resistor R_{sensor} (Figure 4.2). Since the current source designed by the other subgroup is not completely load independent [2], the resistor must not add too much load to the tissue-load. However, decreasing the value of R_{sensor} will decrease the accuracy of the the current detector since a smaller voltage drop is more difficult to determine accurately due to noise on the signal. The value of R_{sensor} is chosen to be 200 Ω, which will cause a voltage drop of 3 V when 15 mA is put into the tissue.

Voltage Divider

The voltage at $input_+$ is expected to be as high $10.5 + \mathrm{V}_{CC} + \mathrm{V}_{\mathrm{R}_{sense}} = 14$ V. Because the voltage after the coupling capacitor is limited on 10.5 V and the voltage drop over the coupling capacitor will not become higher than 0.5 V (chapter 5). Since the input buffers will be powered with +15 V single-supply voltage, the voltage is divided at both inputs by 2 to guarantee a right output of the input buffers. The voltages are divided by using two 100 kΩ resistors. Thus, the expected maximum input voltage is calculated using Equation 4.1. The calculated maximum buffer input voltage is 7 V.

$$\left(\frac{10.5 + V_{CC} + V_{R_{sense}}}{2}\right) = 7 \text{ V} \tag{4.1}$$

Input Buffers

For the input buffer operational amplifiers (op-amps), the important characteristics are a high input impedance, a precise unity gain and the ability to follow the input voltage range accurately, also single supply operation is required. The high input impedance will not influence the voltage divider at the input and a precise unity gain is needed for an accurate

output signal. Taken this into account the ICL7612 of Intersil was chosen. The ICL7612 has an input impedance of 1 TΩ, an unity gain bandwidth of 0.48 MHz and a slew rate as high as 1.6 V/μs, which provides fast voltage following [28].

Differential Amplifier

The next component to implement was the differential amplifier. The accuracy of the differential amplifier for unity gain is dependent on the matching of the resistors around the op-amp. Therefore, dedicated differential amplifiers are produced with the resistors build in the IC. Since the current through R_{sensor} can be positive and negative, the differential output voltage of the buffer stage can also be positive as well as negative. In order to let the differential amplifier operate on single supply voltage, an offset of 5 V is put on the signal. For this application, the INA117P of Texas Instruments was chosen because it has a precise unity gain (error of max 0.05% [29]). The offset on the differential signal is achieved by supplying the required offset voltage to the ref pin of the INA117P [29].

Inverter

For the inverter, an op-amp with precise unity gain and two resistors that are identical are needed. It is important to notice that the signal needs to be inverted around +5 V, thus the non-inverting input of the op-amp is connected to the offset voltage. The needed op-amp characteristics were almost identical as for the input buffers, therefore the ICL7612 will also be used as inverter. For the resistors, two 10 kΩ resistors with 0.1% tolerance have been chosen.

Comparators

Lastly, the right comparators need to be chosen. The reference voltage for the comparators will be 6.5 V, since the signal is now increased with an offset of 5 V. The output has to switch between 'logic low' and 'logic high' for the OR-gate of the error module. For this application, the LM211 of Texas Instruments [30] was chosen. It has an typical offset voltage of 0.7 mV, which is the difference in input voltage needed to trigger a high output and it can operate on a +15 V single supply voltage. The LM211 has an open collector output which can be pulled up to the desired voltage using a voltage source and a resistor. In Figure 4.3, the configuration of the LM211 can be seen. When V_{in} becomes higher than V_{ref}, the output is pulled up to V_{DD}. V_{DD} is set to 5 V for this application.

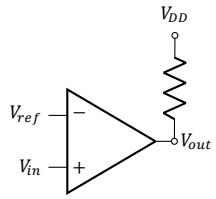

Figure 4.3: Comparator configuration.

4.2.2. Implementation of the Overvoltage Detector

Differences With Respect to the Overcurrent Detector

If the same implementation as the overcurrent detector would be used for the overvoltage detector, there are two problems. When the fault condition of -10.5 V over the tissue would occur, the differential voltage input of the differential amplifier would be -5.25 V. Thus, an offset voltage of 5 V would not be enough to let the differential amplifier operate at single supply voltage. The other problem is that V_{ref} should be adjusted. Both problems were solved by changing the ratio of the voltage divider. The divider for the overvoltage detector consists of a 107 kΩ and a 17.8 kΩ resistor. Now the differential input at the differential amplifier in case of -10.5 V over the tissue will be -1.5 V. In this case, the 5 V offset is sufficient. Since the differential voltage will be 1.5 V, the reference voltage of the comparators can also be kept on 6.5 V.

4.2.3. Simulations of the Detector Sub Modules

After component selection, both detectors were simulated using LT Spice. There was no spice model found for the ICL7612, therefore the simulations are done with the standard *Universal op-amp 2* spice model. Two types of simulations have been done, to test the trigger levels and to test the signal response. In Figure 4.4 the trigger levels of both systems are simulated. In Figure 4.4a a DC sweep of the voltage over the tissue between 10.3 V and 10.7 V is done. In Figure 4.4b a DC sweep of the current through R_{sensor} between 14.5 and 15.5 mA is done. As can be seen, the error outputs trigger on 10.54 V and 15.09 mA, the offset is due to the offset that is needed to trigger the comparators.
In Figure 4.5a a pulse of 10.8 mA with a pulse width of 20 μs and a inter pulse delay of 30 μs at a frequency of 10 kHz is put through a tissue load of 1 kΩ. In Figure 4.5b a biphasic stimulation pulse with an amplitude of 16.5 mA, pulse width of 20 μs and inter pulse delay of 30 μs at a frequency of 10 kHz is simulated. As can be seen, the error signal has a delay on the input of the module. This is due to the slew rate of the INA117P. Due to the slew rate of the ICL7612, the input buffers will also have this delay. Since the current pulses created by the waveform subgroup will have a certain rise time [2], this delay is not considered to be any problem.

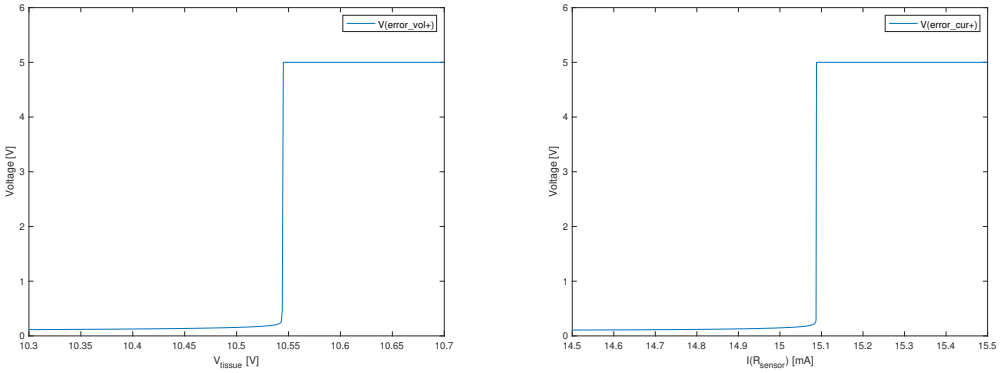

(a) (b)

Figure 4.4: Output signal of the (a) overvoltage detector on tissue voltage and (b) of the overcurrent detector on current through R_{sensor}. The output signal triggers for (a) at input voltage of 10.54 V due to offset voltages and (b) a input current of 15.08 mA due to offset voltages of the comparators. Simulation of the output signal of the detection circuits (Figure 4.1, Figure 4.2). The input voltage is swept around the designed trigger voltages.

4.3. Prototype of the Detector Sub Modules

After simulating, the sub modules were tested on proper functioning. For these measurements the sub modules were supplied by an ISO-TECH IPS-4303 DC power supply and the signals were measured with a Tektronix TDS 2014C oscilloscope. Input signals were generated using a HP 3310B function generator.

4.3.1. Pulse Responses

First, the pulse response of both sub modules was tested. The overcurrent detector circuit was tested by putting a 33 μs (15 kHz) pulse of 3.1 V directly over R_{sensor} creating current pulses of 15.5 mA, in Figure 4.6a the result of this measurement can be seen. The overvoltage detector circuit was tested by putting a 33 μs (15 kHz) pulse of 11 V over the module input terminals, in Figure 4.6b the result of this measurement can be seen. As expected, both modules show a delay around 3 μs.

4.3.2. Trigger Voltages

For the measurement of the pulse responses in Figure 4.6, the input voltages were set slightly above the set trigger voltages. This was done because the modules showed a noisy output

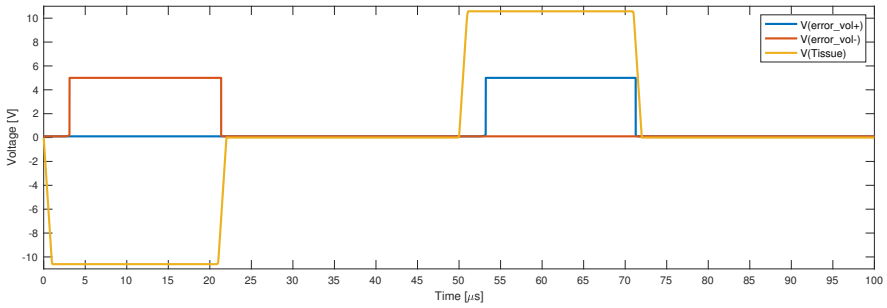

(a)

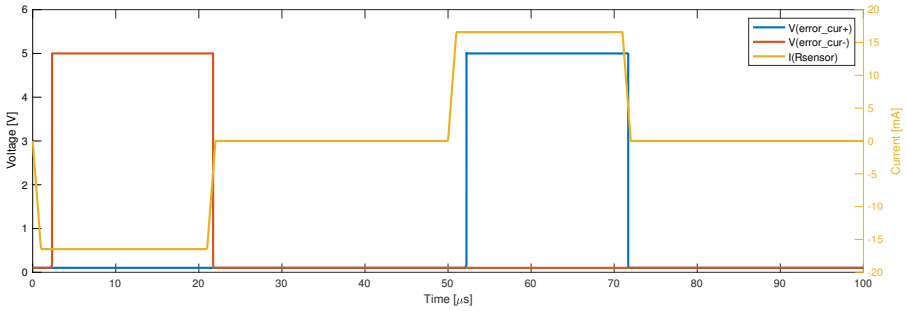

(b)

Figure 4.5: Simulation of (a) the overvoltage detector and (b) the overcurrent detector. In (a), the output signal $error\_vol-$ is set high 2μs after the input signal exceeds -10.5 V. Output signal $error\_vol+$ is set high 2μs after the input signal exceeds 10.5 V. In (b), the output signal $error\_cur-$ is set high 2μs after the input signal exceeds -15 mA. Output signal $error\_cur+$ is set high 2μs after the input signal exceeds 15 mA.

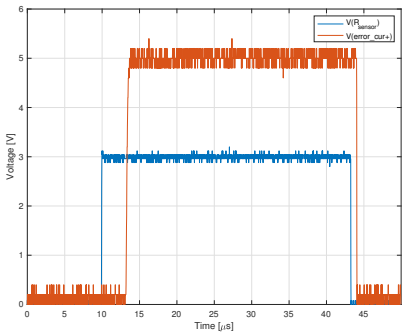

(a)

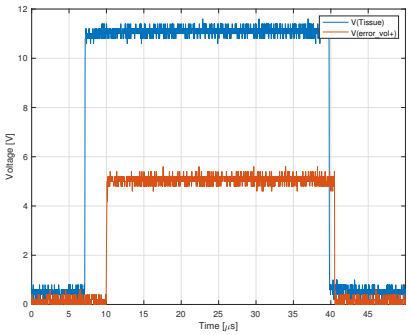

(b)

Figure 4.6: Pulse response of (a) the overcurrent detector and (b) the overvoltage detector at 15 kHz. Both (a) and (b) outputs show a delay with respect to the input signal, as is expected from the simulations.

signal when tested with the designed voltages, which was expected from the simulations. Therefore, the trigger voltages of both modules was measured by putting a low frequency triangular pulse around the trigger levels on the modules. The results of these measurements can be seen in Figure 4.7. This measurement shows that indeed the overcurrent detector triggers slightly above 3.0 V and that the overvoltage detector triggers around 11.0 V. This has to do with inaccuracies in the voltage dividers and the input offset that is needed for the comparators.

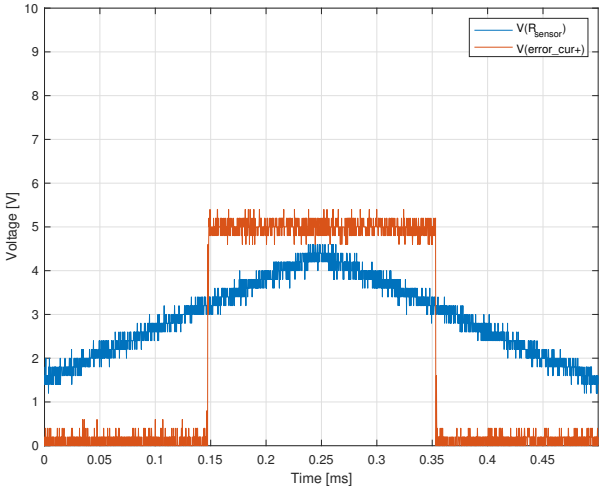

(a)

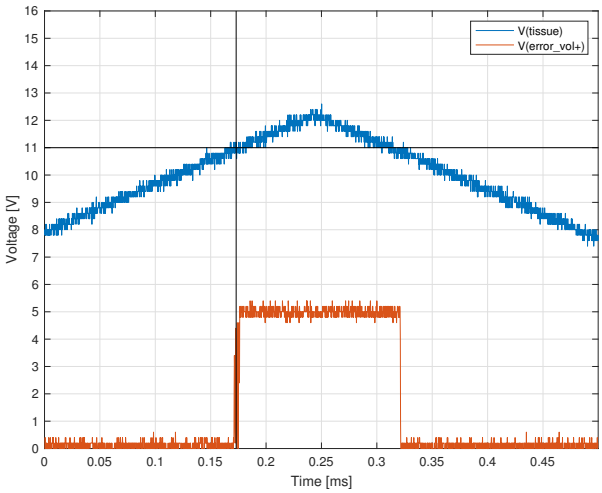

(b)

Figure 4.7: Measured trigger voltage of (a) the implemented overcurrent detector and (b) the implemented overvoltage detector. Due to the noisy signal it is difficult to determine the exact trigger voltage. As expected in (a) the trigger voltage in is higher than the designed 3.0 V and in (b) the trigger voltage is higher than the designed 10.5 V.

5

Coupling Capacitor

This chapter covers the design and implementation of a coupling capacitor which gets rid of the DC signal of the stimulation waveform. This prevents harmful stimulation as discussed in subsection 1.2.4.

5.1. Possible Designs for the Couping Capacitor

This section covers possible designs that can be considered when implementing the coupling capacitor. Both a single coupling capacitor and high frequency current switching design are discussed.

5.1.1. Single Coupling Capacitor

To block DC signal, a single coupling capacitor as shown in Figure 5.1 can be used. This is the conventional way as described in literature [25].
The signal generated in the neural stimulator is a waveform with either a low or high frequency. The waveform is often a square wave as it allows for easy charge injection measurements [15]. For the neural stimulator that is designed during this project, the device will primarily focus on stimulating between the frequency of 1 kHz and 15 kHz [1, 2]. The coupling capacitor will have to be selected such that it can work with these frequencies. The size of the coupling capacitor is dependent on the amount of charge delivered per cycle. Equation 5.1 can be used to determine the size of the coupling capacitor [25].

$$C = \frac{Q}{V} = \frac{I \cdot t}{V} \tag{5.1}$$

Equation 5.1 shows the relation between stimulation current amplitude I, the time t, the voltage drop over the capacitor V and the required capacitance C. To limit the voltage drop over the capacitor, often a coupling capacitor with high capacitance is required [31].

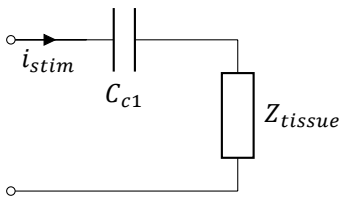

Figure 5.1: Basic coupling capacitor topology.

5.1.2. High Frequency Current Switching

Conventional single coupling capacitors usually have a large size. High frequency current switching (HFCS) can be used to reduce the size of the coupling capacitor [25]. Instead of

having a single high capacitance coupling capacitor which block the DC signal, two lower capacitance capacitors are used. These capacitors are switched with a very high frequency, this way a capacitor can block the DC signal for a small period of time and can then discharge while the other capacitor blocks the DC signal [31, 32]. This method is independent of the stimulation frequency, so it does not matter whether the neural stimulator stimulates with 10 Hz or 1kHz. The two capacitors switch at a higher frequency causing charging and discharging to happen in shorter time periods. The circuit topology for HFCS found in literature [25] was found to be only suitable for monophasic stimulation.
For the designed neural stimulator, it is a requirement to support biphasic stimulation which requires changes to the topology presented in [25]. It has been looked into extending the monophasic topology for biphasic stimulation. This added complexity to the topology and had too much overhead. The designed topology can be found in appendix A.1.
HFCS is an interesting alternative to the conventional coupling capacitor, since it is a method which is frequency independent and allows for smaller capacitors. However, the current implementations of HFCS are not suitable for biphasic stimulation and the complexity of implementing this was too high for this project.

5.2. Implementation of Coupling Capacitor Sub Module

For the designed neural stimulator, size is not an issue and discrete components can be used. Therefore, a single coupling capacitor is used for the neural stimulator. For the implementation of this coupling capacitor there are two main considerations: the size of the coupling capacitors and the type of capacitor.

Coupling Capacitor Size

Equation 5.1 shows the equation to calculate the size of a coupling capacitor. For this equation, the parameters for high frequency stimulation are initially chosen. The most charge buildup will happen with a stimulation of 1 kHz at 10 mA [1, 2]. With 1 kHz, the maximum possible stimulation duty cycle is 0.5 ms. The maximum voltage drop over a single capacitor has been set to 0.5 V. A small voltage drop over the coupling capacitors will allow for larger tissue loads which is favourable. Using Equation 5.1, the needed capacitance is calculated to be 10 μF.

Type of Capacitor

For the type of capacitor, research has been done to medically graded capacitors [33]. These medically graded components have extensive quality tests which results in high reliability. They are therefore suitable for application in a neural stimulator. Additionally, the polarity of the capacitor is important since the entire neural stimulator will operate between 0 and 15 V [1, 2]. A non-polarised capacitor is required due to the biphasic stimulation.

Chosen Capacitor

With the considerations for type and size, the AVX 12103C106K4Z2A coupling capacitor [34] has been chosen. No medically graded non polarized capacitor could be found. The AVX matches the size requirements, is non polarized, and has Automotive Electrical Council(AEC) Q200 qualification[35]. As it is not possible to simulate the specific capacitor, no simulations are presented in this chapter.

5.3. Prototype of the Coupling Capacitor Sub Module

The circuit has been built with the AVX 12103C106K4Z2A. This circuit includes the voltage detector of chapter 4, the JFET of chapter 6 and NMOS of chapter 8. This leaded to the circuit seen in Figure 5.2. The HP 3310B function generator has been used to generate an input signal for the circuit with a resistor as load and the voltage relative to ground was measured using the Tektronix TDS 2014C oscilloscope. While testing, the offset was increased. The results can be seen in Figure 5.3. Figure 5.3 shows that not all the offset is gotten rid off as the signal is fluctuating between -1V and a higher positive amplitude. This is caused by the added components between the coupling capacitor and electrode. In the anodic phase, when

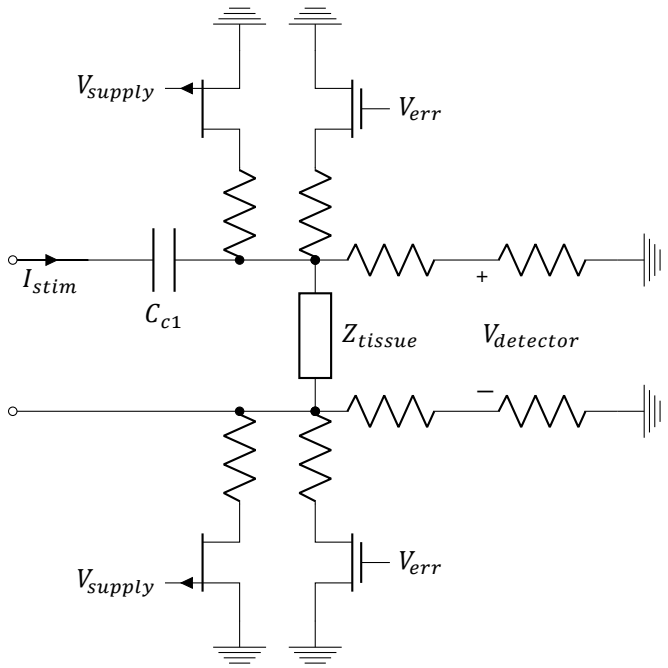

Figure 5.2: The circuit with which the coupling capacitor sub module is tested, the coupling capacitor is combined with the voltage detector, single fault safety and error sub modules.

I_{stim} as indicated in Figure 5.2 has a negative current, a DC offset can be introduced and is therefore not blocked. This problem is discussed in chapter 10 and a possible solution is presented.

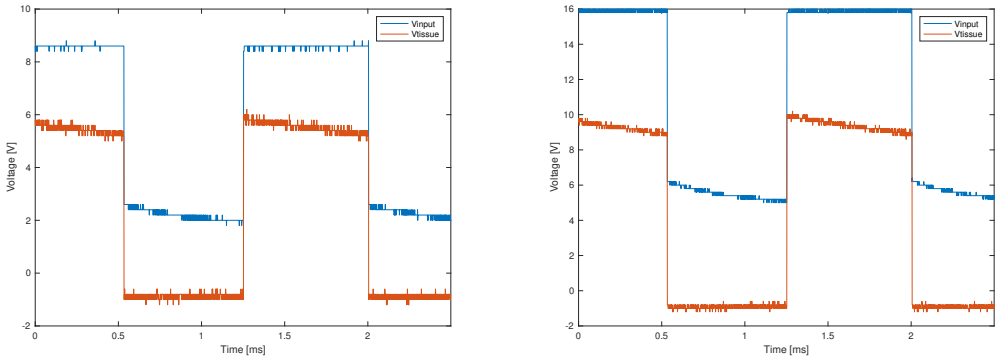

(a) (b)

Figure 5.3: Result of the coupling capacitor circuit with offset. (a) shows the testing result with a relatively small and (b) with a larger DC offset. It can be seen that not the complete DC offset is filtered from the signal because V_{tissue} still has a DC offset.

6

Single Fault Safety

In the program of requirements, single fault safety was described as the safe power-off of the system. For our device, the safety module should discharge any charge that was put into the tissue at the moment of powering off, to prevent the situation in which the stimulation is stopped halfway and an amount of charge is stored in the tissue. In order to fulfil this, two discharge switches were implemented, which short the tissue to ground in case the power supply shuts down.

6.1. Design of the Single Fault Safety Sub Module

To meet the set requirements, two switches are placed, one on both sides of the tissue to ground. When the switches close, both sides of the tissue are grounded and thereby the tissue will be discharged. For the design of the switch, it was chosen to use JFET transistors. JFET's are depletion mode devices and therefore a V_{GS} of 0 V will put the transistor in it's ohmic region. The gate of the JFET will be controlled via one of the 15 V power supplies, which goes to 0 V when the system is turned off and the source will be connected to ground. To protect the tissue from the supply voltage in case the transistor breaks down, resistors (R_3 & R_4) are placed between the power supply and the gates of the transistors. Lastly, resistors (R_1 & R_2) are placed between the tissue terminals and the transistor drain inputs to limit the maximum current that will flow when the switches are closed. The circuit topology can be seen in Figure 6.1.

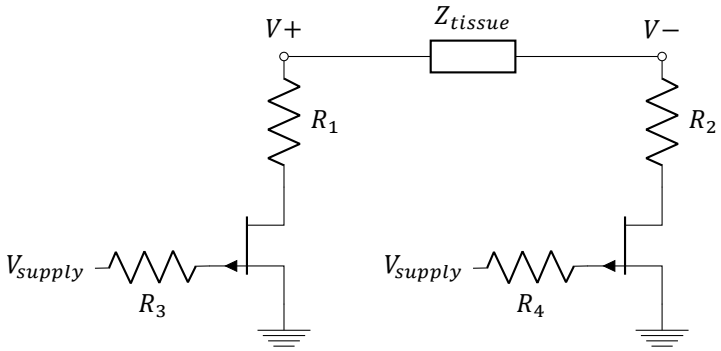

Figure 6.1: Topology of single fault safety switches.

6.2. Implementation of the Single Fault Safety Sub Module

For the implementation of the switches, the JFET and resistor values had to be chosen.

6.2.1. Selected Components

JFET

The JFET is going to be controlled with the supply voltage, thus a positive voltage (with respect to the source) will be put on the gate to turn the transistor off. A p-channel JFET is needed for this functionality. The breakdown voltage must be higher than 15 V, the transistor should be in the cut-off region when 15 V is applied to the gate and the max gate-source voltage should also be higher than 15 V. The J176 was chosen for this application. It has a breakdown voltage of 30 V, $V_{GS,max}$ of 30 V and a cutoff gate-source voltage of 1.0 V [36].

Resistors

For resistors R_1 & R_2, a value of 1.5 kΩ is chosen to limit the discharge current to 10 mA when 15 V is present at the terminal at the moment of discharging.

$$R = \frac{V}{I} = \frac{15V}{10mA} = 1.5\,\text{k}\Omega \tag{6.1}$$

For the resistors R_3 & R_4, a value of 100 kΩ was chosen in order to limit the current to 100 μA in case the transistor breaks down. These transistors would ideally be as big as possible, however the small reverse gate current of 1 nA [36] of the transistors will induce a voltage drop over the resistors. When the resistors are in the megaohm range, this voltage drop is more than 1 V. A lower gate voltage limits the drain voltage because of the threshold voltage of the transistor.

6.2.2. Simulations

To test the discharge capability of the single fault safety switches, simulations were done using LT Spice. In the simulation a 10 mA current pulse of 10 μs was put into a 10 nF capacitor parallel to a 100 kΩ resistor, creating a potential difference of 10.9 V. After 100 μs V_{supply} was turned off, closing the switches. The simulation results can be seen in Figure 6.2. As can be seen, the capacitor discharges very slowly until the switches are closed. 252.5 μs after closing the switches, the potential difference over the capacitor is just 2.9 mV.

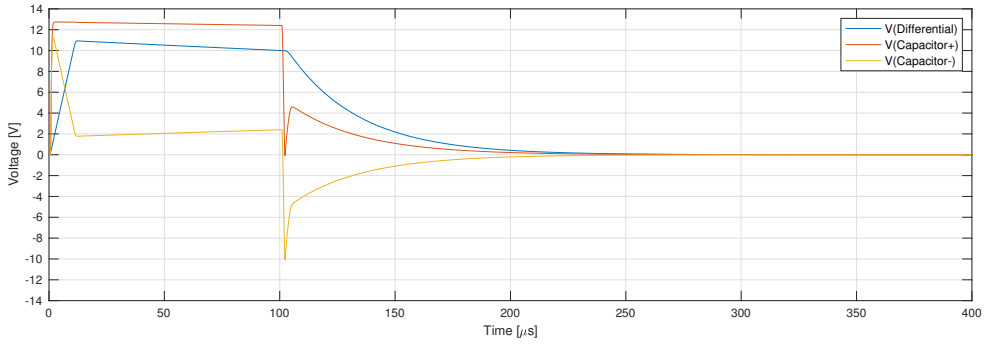

Figure 6.2: Simulation of single fault safety switches discharging a 10nF capacitor. The capacitor is charged up to a voltage of 10.9 V. For the first 100μs, the single fault safety transistors are kept in cut-off region to show the discharge of the capacitor. After 100μs, the single fault safety switch is closed. Accelerated discharging can be seen in the figure. After 352.5μs, the voltage over the capacitor is dropped to 2.9 mV.

6.3. Prototype of the Single Fault Safety Sub Module

The proper working of the single fault safety switches was tested during saline solution measurements on the total system, this will be discussed in chapter 9.

7 Charge Integrator

To detect the charge present at the electrode surface when stimulating with the neural stimulator, a charge integrator is used. Dangerous charge levels need to be detected and it is favourable to have charge balance in the tissue [37]. Different topologies can be used to monitor the charge injected. Possible designs will be discussed, of which one will be chosen. Then a prototype of the chosen design is made.

7.1. Possible Designs for the Charge Integrator Sub Module

The possible topologies which can be used to integrate the charge that will be considered in this chapter are a passive capacitor integrator, a high frequency current sampler and voltage detection over the tissue.

7.1.1. Passive Current Integrator

One way to measure charge is by using a passive current integrator as shown in Figure 7.1. This integrator is to be connected between two terminals through which the integration current flows [11]. The current through the capacitor charges the capacitor and this results in a voltage difference over the capacitor. This voltage is linearly related to the current through the capacitor and is measured and buffered by a differential amplifier. The output of the differential amplifier is then compared with a reference voltage to check whether the amount of charge at the electrode interface is reaching dangerous levels or if there is charge balance [11]. When charging and discharging a capacitor, it is possible that an error signal is triggered in the system. In these cases the capacitor must discharge and reset using the switches.
The capacitor in Figure 7.1 is floating, therefore it is difficult to discharge the capacitance by a single transistor. The operating range of the neural stimulator is between 0 and 15 V and so is the operating range of the charge integrator. To discharge the capacitor, transistors can be used.
The passive charge integrator is implemented in the designed neural stimulator. For the implementation of this topology, a mirror of the current will be needed. The additional capacitance can not be put in series with the electrode as this adds too much load [11].

7.1.2. High Frequency Sampling

Another way to measure the charge that is stimulated into the body, is by measuring the current using high frequency sampling. By measuring the current with a high frequency, the current which goes into the body can be measured and the microcontroller can then calculate the amount of charge which enters the body. The measurements from the current detector described in chapter 4 could be used. These calculations will have to be done rapidly by the microcontroller. This microcontroller would also have to act independently of the microcontroller used by the interface and waveform subsystems [1, 2] since interrupts could result into dangerous stimulation parameters.

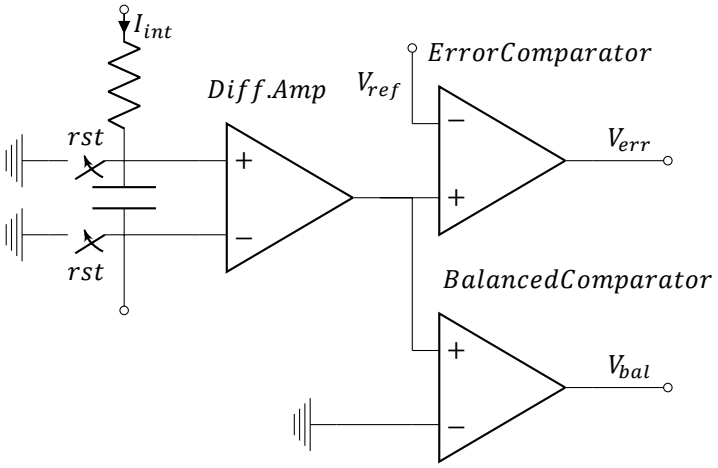

Figure 7.1: Passive Current integrator topology.

High frequency sampling would require a lot of computations to be done and can cause errors due to interrupts. Therefore it is not implemented in the designed neural stimulator

7.1.3. Voltage Measurement Over the Tissue

Charge balance can be achieved by measuring the voltage over the tissue. For this, the voltage detector described in chapter 4 can be used when there is no stimulation present. If there is charge left in the tissue, a voltage can be measured with the voltage detector. The measured charge can then be compensated. An active method to balance the charge is to measure the voltage and add short pulses after a symmetric cathodic/anodic stimulation. As long as the voltage over the tissue is not within a specified range, these pulses will continuously be given [37]. For the designed neural stimulator, this is difficult to implement due to the high frequency and the allowed duty cycle of the designed neural stimulator.
Another charge balancing method is to shorten the anodic phase of the waveform based on the voltage over the tissue. It is difficult to provide feedback on the charge in the tissue when stimulating. Additionally, it is difficult to determine how much shorter the anodic phase should be to cancel out the voltage over the tissue. In order to do this accurately, knowledge is needed about the tissue, electrode placement and the capacitive value it has.
Measuring the voltage over tissue allows for interesting charge balancing methods, however more research to determine feasibility of these methods at high frequency have to be done before it can be implemented. Therefore it will not be considered in the implemented neural stimulator.

7.2. Implementation of the Charge Integrator Sub Module

The passive charge integrator topology will be implemented. In this section, component choices will be elaborated on and simulations will be presented. It is important to note that for the entire system the operating voltage is between 0 and 15 V.

7.2.1. Implementation Considerations

Charge limiting value

The charge that is built up at the tissue needs to be limited at a value of 30 $\mu C/cm^2$/phase. As it is possible to keep charge at the electrode between phases, it is important to monitor that the value of 30 $\mu C/cm^2$ at the electrode is not exceeded. The electrode used for stimulation is the Medtronic Model 388928 [38], which has an electrode diameter of 1.27 mm and a electrode length of 3mm. This results in an electrode area of 11.96 mm^2 or 0.1196 cm^2.
Therefore, maximum amount of charge at the electrode is allowed to be 30 $\mu C/cm^2 \times 0.1196 cm^2$ = 3.59 μC. Thus the charge at the electrode needs to be limited at 3.59 μC. Since a differential amplifier is used, it is favourable to have the voltage difference over the integrator capacitor

to be as large as possible as this allows for a higher resolution. This high resolution can be created by having a capacitor with small capacitive value. It is preferred to work up to voltage differences of 5 V because of the differential amplifier. An integration capacitor of 1 μF has been chosen. This will put a voltage of 3.59 V over the capacitor in case of dangerous stimulation as shown in Equation 7.1. Thus, an error signal should be generated once there is a differential voltage of 3.59 V over the capacitor.

$$V = \frac{Q}{C} = \frac{3.59 \cdot 10^{-6}}{1 \cdot 10^{-}6} = 3.59V \tag{7.1}$$

Voltage Offset

As the neural stimulator works between 0 and 15 V, an offset at the output of the differential amplifier needs to be introduced to allow successful measurement of a negative voltage over the capacitor. The offset is chosen to be 3.3 V, this signal was already present for the logic circuitry of the board and it allows for sufficient negative voltage over the capacitor.
With this offset, V_{ref} in Figure 7.1 also needs to be increased, therefore the V_{ref} is set to be 3.59 + 3.3 = 6.89 V and the inverting terminal of the *BalancedComparator* is replaced with a signal of 3.3 V.

7.2.2. Selected Components

For the circuit of Figure 7.1, certain choices have been made regarding the components selected, these are as follows.

Capacitor

For the capacitor, a non polarised capacitor is chosen with a value of 1 μF. It is required to have a non polarised capacitor as the current will flow through the capacitor both ways. There were no requirements for size or material. For this, eventually the Panasonic ECWFD2W105J film capacitor was chosen for this application.

Differential Amplifier

The differential amplifier required similar specifications compared to the detector discussed in chapter 4. The requirements for the differential amplifier were: to have resistors build in in the IC, support a single supply, allow a voltage offset to be applied to the output of the differential amplifier and DIP packaging of the amplifier. Since the specifications were quite similar to the differential amplifier in chapter 4, the INA117P of Texas instruments was chosen [29].

Comparator

The requirements for the comparator are similar to those of the detector in chapter 4. The comparator is fed with a single 15V supply and it should be able to handle signals of at least 6.89V. Additionally it was favourable to be able to set the logic voltage freely. Therefore, similarly to chapter 4, the LM211 has been chosen [30].

Reset Transistor

For the reset transistor of the capacitor, transistors with a high switching speed were favoured and a drain-source voltage of at least 15 V was required since the voltage at the capacitor node could not be higher than that. Additionally it was required that the $V_{gs(th)}$ was lower than 5 V so that a logic signal could be used to reset the transistors. Finally, the current going through the transistor will not be higher than 15 mA. The 2N7000 transistor matched these requirements and was therefore chosen to be implemented [39].

7.2.3. Simulations

With the selected components, simulations have been done in LT Spice. For these simulations, a simulated version of the voltage-current converter [1] and H-bridge [2] have been used. Figure 7.2 shows the result of the simulation with a single pulse. V_{diff} is the output of the differential amplifier which measures the two poles of capacitor shown in Figure 7.1. V_{diff}

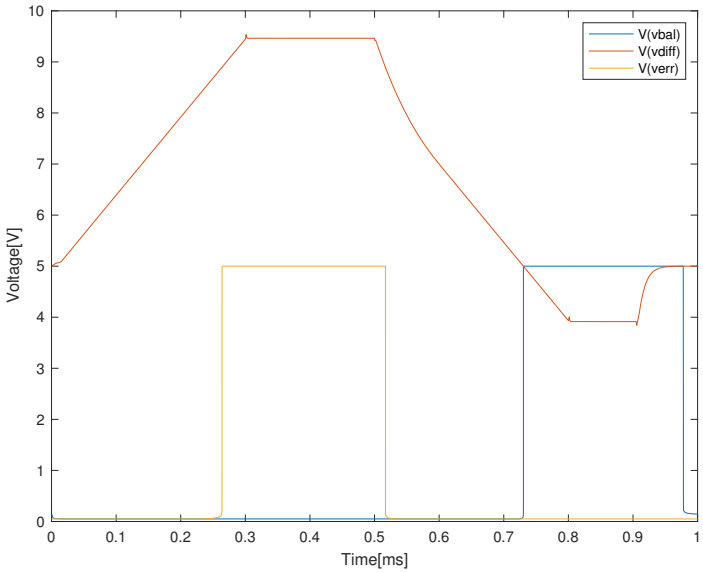

Figure 7.2: Simulation of the charge integrator, both the balanced and error signal are triggered. The stimulation pulse for the simulation is approximately 15 mA for the period 0-0.3 ms and -15 mA for the period 0.5-0.8ms. At 0.9 ms the reset signal is set high. The behaviour of the charge integrator is as expected as the current is integrated during simulation.

has the expected offset of 5V before any stimulation starts. When the reset signal becomes high at 0.9 ms, it can be sensed that the capacitor is discharged. The simulation shows the expected response with the error signal and balanced signal.

7.3. Prototype for the Charge Integrator Sub Module

The final step for the charge integrator made and the design is validated. For the measurements, the prototype was supplied by an ISO-TECH IPS-4303 DC power supply and the signals were measured using a Tektronix TDS 2014C oscilloscope. Input signal was generated using a HP 3310B function generator and a 560 Ω resistor. The results of tests done with both a 1kHz signal and 15 kHz signal can be seen in Figure 7.3. These figures show the input signal $Vinput$, output of the differential amplifier $Vint$, Balanced signal $Vbal$ and Error signal $Verr$. For both frequencies the behaviour is as expected. At 15 kHz, the error signal is not triggered as the charge integrated is not enough to trigger the error signal $Verr$.
The test measurements of the charge integrator with a high reset signal can be seen in Figure 7.4. It can be noticed that the signal is modified, however this is also because the stimulation is still continuing. If the reset for the charge integrator is put on, the stimulation should stop and the capacitor is discharged (as it is also shown in Figure 7.4). This verifies the behaviour of the prototype with the simulation done before.

7.3.1. Trigger voltage

Looking closely at Figure 7.3a, it can be seen that $Verr$ becomes high before $Vint$ reaches a voltage of 6.8 V. The voltage at which $Verr$ is triggered is 3.2V above the offset voltage. This voltage results in a charge of 3.2 μC which equals a charge density of 26.7 $\mu C/cm^2$/phase as shown in Equation 7.2.

$$\frac{3.2\mu C}{0.1196 cm^2} = 26.7\ \mu C/cm^2 \tag{7.2}$$

7.3.2. Current Mirror Mismatch

In the course of the project, it became apparent that the current mirror which is created by the interface subgroup, does not provide a perfect copy of the stimulation current. In order

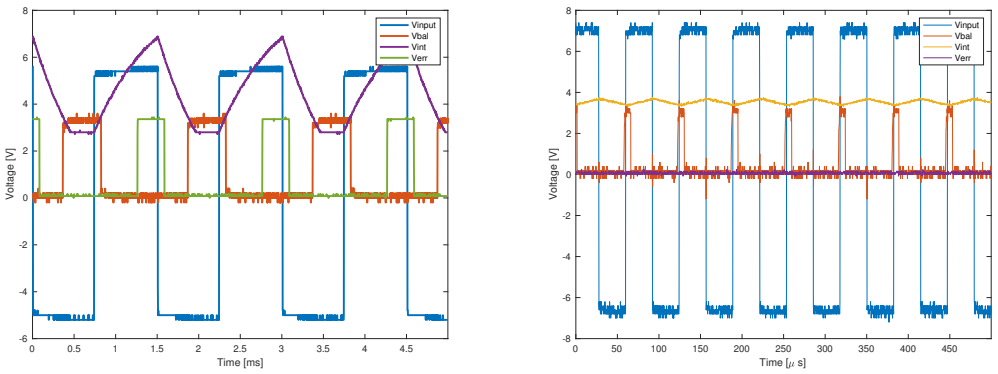

(a) (b)

Figure 7.3: Charge integrator prototype tests at (a) 1 KHz and (b) 15 KHz which both show the expected behaviour. Both comparators show the expected output for both frequencies.

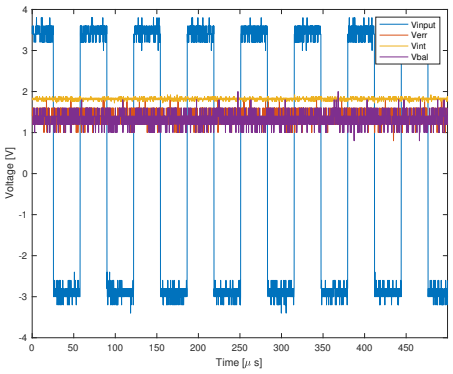

Figure 7.4: Prototype test of charge integrator with high reset signal. As expected the integrated signal is not visible anymore as the current is immediately grounded via the reset transistors.

to achieve a perfect copy, load matching would have to be used. The current mismatch has a maximum deviation of 0.029 mA in simulations [1]. The mismatch does not have serious effect as long as the tissue has an impedance lower than 1400 Ω [1]. As long as the current provided to the charge integrator is higher than the current which is used to stimulate the tissue with, the parameters for dangerous stimulation will have more overhead. In this way, safe charge levels can be guaranteed.
It is possible to correctly balance the wave if the amplitude of the stimulation current is consistently scaled with the integration current. However this balancing becomes more difficult if the stimulation current is not a scaled copy. With the current mirror designed by the interface module [1], the latter is the case. Therefore it is difficult to stimulate the tissue in such a way that there is no charge left in the human body. However, literature has shown that perfect charge balancing is not necessary [15] and the device will only be used for short term stimulation. Severe long term effects can therefore be disregarded.

8

Error Module

As the safety subsystem is generating multiple unsafe stimulation signals, it is important to combine these signals and set the system to a state that will prevent the unsafe stimulation. This error state is not very well defined in the program of requirements, however to prevent current from entering the body, the error state should short the stimulation current.
In total, the error module is concerned with:

- Combining the unsafe stimulation signals
- Setting the error state till a reset is executed
- Closing a switch to discharge the tissue

8.1. Design of the Error Sub Module

To combine the error signals, an OR logic gate will be used. The selected OR gate will have to operate with the voltage of the unsafe stimulation signals outputted by the current, voltage and charge detector.
To set the error state, a flip-flop has to be set. The decision has been made for a Set-Reset (SR) flip-flop [40]. This flip-flop works with inverted signals and can be made to work without a clock. The flip-flop can be implemented using 4 transistors. Table 8.1 shows the behavior of the flip-flop and Figure 8.2 shows the topology of the flip-flop. Since the flip-flop works with inverted signals, an inverter needs to be used between the OR logic gate and flip-flop.
Finally a transistor is required to lead the stimulation current away from the tissue and discharge the tissue in case of an incorrect signal. Together, this leads to the logic system shown in Figure 8.1. This error system handles combining the error signals, setting the error state and discharging the tissue. The output of V_{error} is sent to the H-bridge and the microcontroller to stop further stimulation. For the microcontroller, the signal needs to be below 3.3 V.

8.2. Implementation of the Error Sub Module

The implementation of the error module does not require a specific values to be computed, however suitable components have to be selected.

Table 8.1: Behaviour of SR flip-flop (which works on inverted input signals) [40].

Set	$Reset$	Out	$\overline{Out}$	comments
1	0	0	1	(reset the signal)
1	1	0	1	(after S=1 and R=0)
0	1	1	0	(set the signal)
1	1	1	0	(after S=0 and R=1)
0	0	1	0	(after S=0 and R=1)

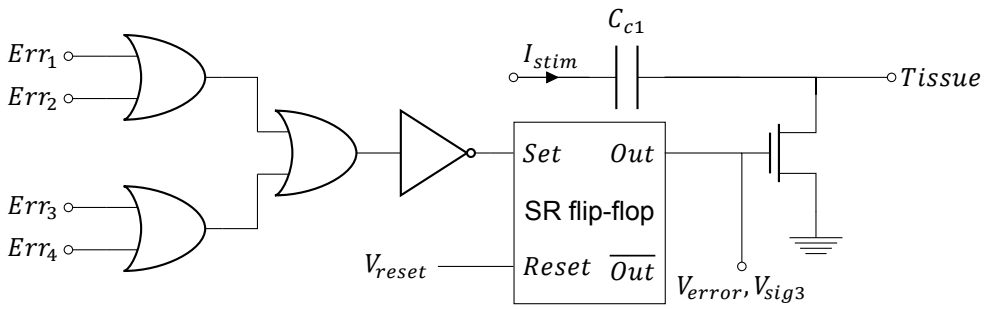

Figure 8.1: Error sub module component overview.

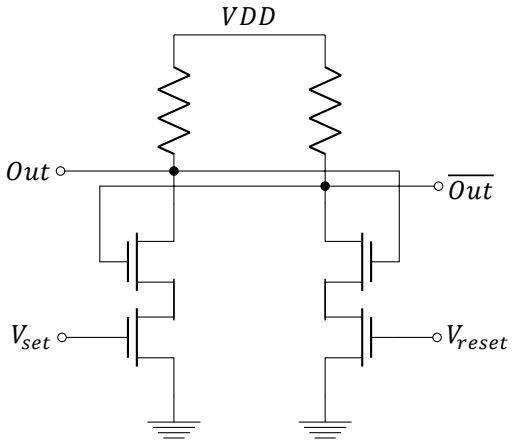

Figure 8.2: Implementation SR flip-flop with transistors.

8.2.1. Selected Components

Transistors

For all transistors in this module, N-Channel MOSFET's are preferred because these are voltage controlled. It was important that the transistors have a high switching speed, can operate within the region of 0-3.3 V, and could handle currents up to 15 mA. For this the 2N7000 transistors were selected [39]. The AEC qualification was not a requirement but should improve the reliability. These transistors can both be found in the inverter, SR flip-flop and the discharging circuit.

OR-Module

The OR-module was selected to be the Texas Instruments CD4072BE. This is a logic OR-module which can combine two inputs to a single output signal. This allows the 3 OR-gates of Figure 8.1 to be combined to a single OR-gate which operates between the voltage of 0-3.3 V. An additional requirement was that the OR-module could operate with a 3.3 V single supply, which the CD4072BE can do [41].

8.2.2. Simulations

The error module was simulated using LT Spice. Since no proper simulation model could be found for the OR-module, only the inverter and SR flip-flop could be tested with the transistor model. For this simulation, the inverter has been implemented and therefore the set signal needs to be 1 to set the flip-flop. There is no inverter for the reset signal, so as shown in Table 8.1, the reset signal needs to be low to reset the SR flip-flop. The simulation results can be seen in Figure 8.3.
This figure shows the desired behaviour aside from the small noisy peaks when the flip-flop switches. Additionally it can be seen in simulation that the switching effect for setting the flip-flop takes 1 μs and resetting the flip-flop takes 2 μs. When using this output signal to drive the transistor behind the capacitor on Figure 8.1 this should cause no problem. When

feeding the signal back to the microcontroller [1, 2], it is important that the signal stays below 3.3 V.

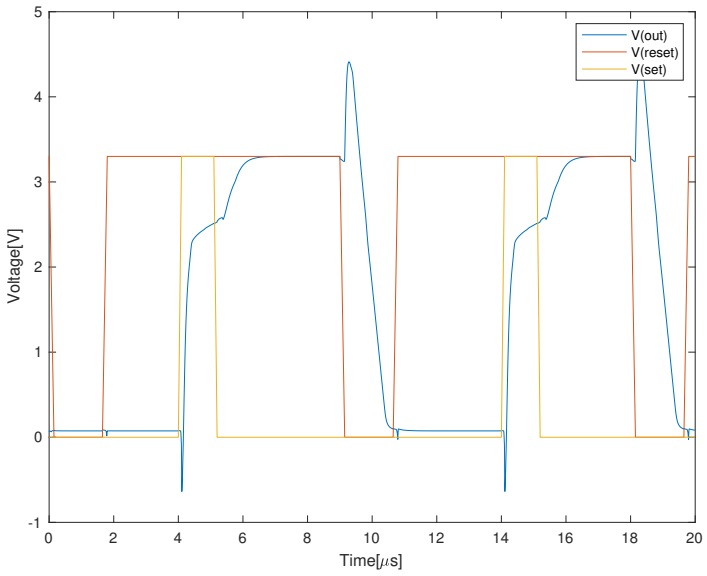

Figure 8.3: Simulation of SR flip-flop made with 2N7000's. The flip-flop shows the behaviour described in Table 8.1 when the set signal is high and the reset signal is low. Switching effects on the output can be seen when the signal is reset.

8.3. Prototype of the Error Sub Module

A prototype of the error module has been made with the components described in subsection 8.2.1. This circuit has been implemented and tested. The expected output of 3.3 V is delivered by the flip-flop. To see if the circuit was behaving as expected, it was connected to the ISO-TECH IPS-4303 DC power supply which was set to 3.3 V. Before starting the test, the system is first reset. Then via the supply, an input signal is given to one of the four error inputs shown in Figure 8.1 and afterwards the SR flip-flop was reset. The switching effects have been measured via the Tektronix TDS 2014C oscilloscope. As seen in Figure 8.4, the switching effect is not visible. This is desirable for the flip-flop. Figure 8.1 does not allow analysis of the switching effect and therefore no remarks can be made about the switching delay of the prototype.

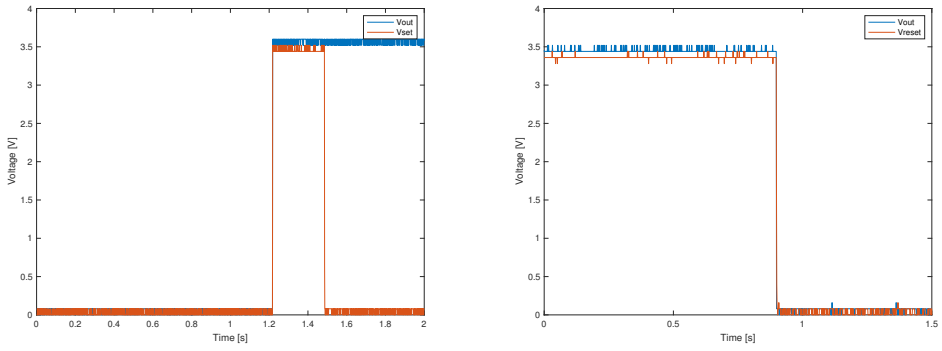

(a) (b)

Figure 8.4: Pulse response the error module showing the behaviour described in Table 8.1. In (a), the error module is set with a 3.3 V signal on one of the OR inputs and the flip-flop is sucessfully set to a *logic high* signal. In (b), the error module is reset by grounding the reset signal and the output of the flip-flop is successfully set to a *logic low* signal.

9 Measurements

After combining all designed sub modules, a measurement setup was made with the complete SYSTEM. The aim of the measurements was to prove the discharging capability of the safety module after a period of stimulation.

9.1. Method

To simulate the electrical characteristics of nerve tissue, 1 tablet of 'P4417 Phosphate buffered saline' from Sigma-aldrich was dissolved in 200 mL of deionized water resulting in a 0.01 M phosphate buffer, 0.0027 M potassium chloride and 0.137 M sodium chloride solution. The stimulation device was connected to electrode 0 and 1 of a Medtronic model 3889 electrode lead, which was put in the saline solution. To determine the built up charge in the tissue, the voltage over the electrodes was measured. For the measurement, the safety module was powered using a TENMA 72-8695 DC power supply, the input signal came from the implemented waveform module which was powered by a 9 V battery and the voltage over the electrodes was measured using a HP 3458A Digital Multimeter.

9.2. Results

In this measurement, the effect of using the single fault safety to discharge the solution was measured. Two different measurements were done. First, a stimulation signal of 10 mA at 1 kHz was applied to the electrode. After 3 minutes, the electrode was disconnected from the stimulation device and the voltage over the electrode was measured every 10 seconds over a period of 2 minutes. This measurement was repeated three times.
After that, the electrode was again stimulated 3 minutes using a 10 mA, 1 kHz signal but now the stimulation devices was turned off after three minutes. Again, the voltage over the electrode was measured every 10 seconds over a period of 2 minutes and the measurement was repeated three times. The difference in the measurements was that by turning off the stimulation device, the single fault safety switches were closed. The measured voltages are plotted in Figure 9.1 and clearly show how the single fault safety switch helps discharge the tissue faster.

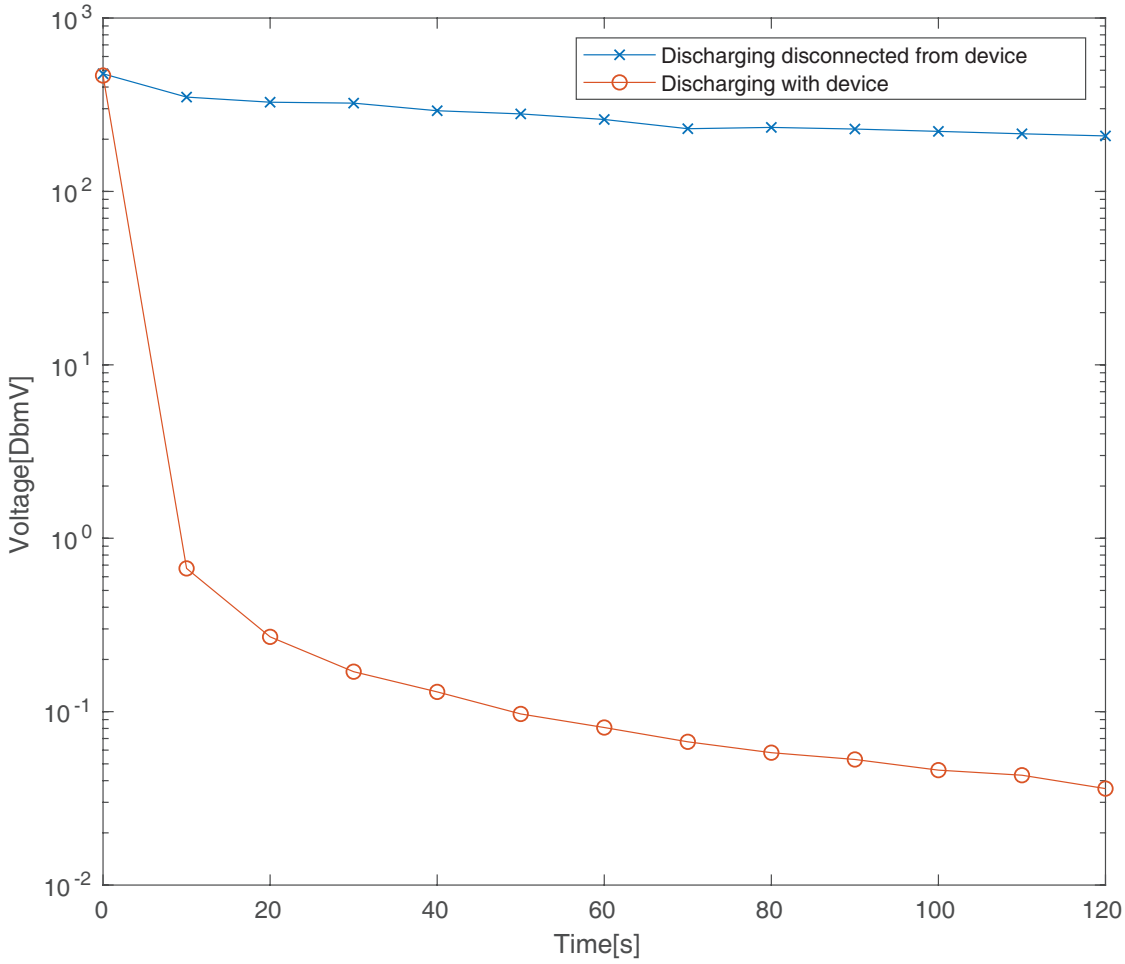

Figure 9.1: Logarithmic plot of the discharge of a 0.01 M phosphate buffer, 0.0027 M potassium chloride and 0.137 M sodium chloride solution after a stimulation period of 3 minutes at an amplitude of 10 mA at 1 kHz. The figure shows clear improvement of the discharging when the device stays connected to the electrode after the stimulation period, which shows the functioning of the single fault safety switches.

10 Discussion

In this chapter, the achieved results will be discussed for validity and possible improvements will be proposed.

10.1. Reliability of Components

The qualification of the used components has been looked in to. There is no medical standard for electrical components, only the IEC60601 is present which specifies the basic safety and essential performance of medical electrical equipment [42]. There are components which are 'Medical grade' and promise high reliability [34].
Aside from the medical grade, there is also the Automotive Electronic Council (AEC) qualifications. Components with these qualifications can safely be used in harsh automotive environments without additional qualification or testing. There are multiple variations of the qualifications. For our neural stimulator, the AEC-Q101 [43], which concerns the failure mechanism based stress test qualification for discrete semiconductors and the AEC-Q200 [35], which concerns the stress test qualification for passive components are relevant.
For the IC's that have been used in the safety module, qualifications have been searched and can be found in Table A.1 in appendix A.2. Most components do not have a qualification, for these cases the reliability is defined by the manufacturing company. For Texas instruments, the reliability is set to have less than 50 failures in time at 100,000 power on hours at 105°C. Additionally, the test methodologies performed by Texas instruments is according to the Join Electron Devices Engineering Council (known as JEDEC) [44].
Intersil has reliability tests available on their website which show that the Intersil ICL7612 has 0 rejects when recent stress tests [45]. ON Semiconductors also provides reliability data per component and for both the J176 and 2N7000 the equivalent device-hours are above 250 million hours [46].
Statistically seen, it is always possible that a component fails. Qualifications like the AEC qualification can give extra trust in the correct functioning of a component and even without the qualifications, companies consider reliability very important and the equivalent device hours for the J176 and 2N7000 are good illustrations of that.

10.2. Accuracy of the Safety Module

The detectors and charge integrator sub modules were designed with ideal parameters in mind. However, during testing of the prototype it became clear that delays and inaccuracies of the physical components introduced small inaccuracies on the trigger voltages. As stated in section section 4.3, the inaccuracies cause the detectors to trigger above the set safety limits. To fulfil the requirement that currents above 15 mA and voltages above 10.5 V should be prevented, it is recommended to lower the voltage V_{ref} in the final design so that the detectors will stop the stimulation before the safety limits are exceeded. It is not expected that this will influence the functioning of the complete device since the safety limits are higher than the required parameters as set by the waveform subgroup [2]. The charge integrator

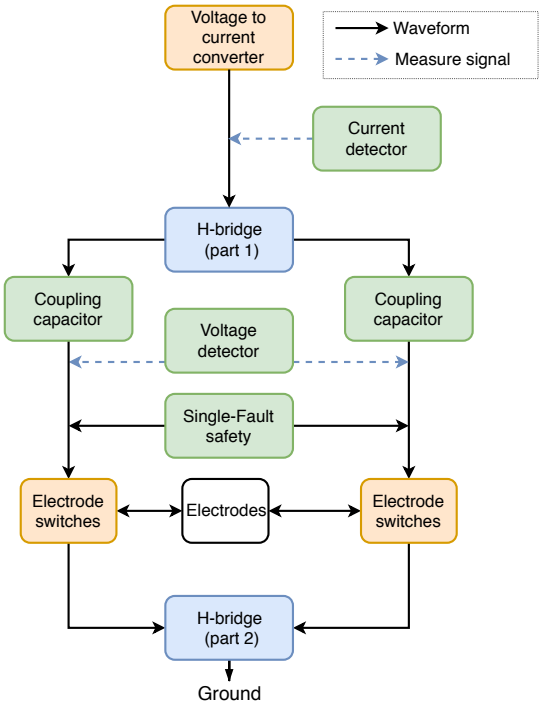

Figure 10.1: Possible layout for a double coupling capacitor circuit, blocking both anodic as cathodic DC offset signals.

triggers before the safety limit of 30 $\mu C/cm^2$ is exceeded due to inaccuracies in the prototype. This meets the requirement that charges above 30 $\mu C/cm^2$ at the surface of the electrodes must be prevented, therefore the inaccuracies are seen as an advantage in this case.

10.3. DC Blockage of the Safety Module

In existing literature, the topologies found for biphasic stimulation show the use of a single coupling capacitor [23, 25]. This is in cases where there is only an electrode behind the coupling capacitor. However, as can be seen in the module overview in Figure 3.3, the designed neural stimulator also has components between the coupling capacitor and the electrodes. The components after the coupling capacitor are able to provide a path to ground, which prevents the DC blockage in the anodic pulse. Moving the coupling capacitor to just before the electrode would solve this issue, however this would affect the functioning of the voltage detector and influence the discharging of the tissue [47]. Figure 10.1 shows an alternative implementation which should block the complete DC current without losing any of the functionality of the current or voltage detectors. This system has not been tested due to time constraints, however this is expected to solve the DC current problem for both the cathodic and anodic phase.

10.4. Discharging of the Tissue

During measurements, the discharging of the electrodes at system shut down was shown. However, with the proposed change of location for the coupling capacitor the discharge behaviour of the tissue could change. New measurements should be done with the new location of the coupling capacitor.

11

Conclusion and Recommendations

11.1. Conclusion

Concluding, this thesis described the design process of a safety module for an arbitrary waveform generator to be used as neural stimulator. To meet all the set requirements in chapter 2, the system was devided into multiple sub modules.
To prevent voltages higher than 10.5 V to be put over the tissue, an overvoltage detector was designed. The implemented prototype is able to protect the tissue from voltages higher than 11 V, but with the proposed improvement, voltages above 10.5 V can be detected.
To prevent currents higher than 15 mA to be put into the tissue, an overcurrent detector was designed. The implemented prototype is able to protect the tissue from currents higher than 15.5 mA, but with the proposed improvement this detector is also able to meet the specified requirements.
The implemented coupling capacitor does not function as desired, as it is not able to block the complete DC offset of an input signal. This is due to the different subsystems being present behind the coupling capacitor allowing a DC offset to be introduced in the anodic phase. This problem has been discussed in chapter 10 and a possible solution is presented.
To ensure the discharge of the tissue when shutting down the system, two single fault safety switches were implemented. The functioning of these switches was verified during the measurements in chapter 9.
To prevent charges higher than 30 $\mu C/cm^2$ at the electrode tissue interface, a charge integrator was designed. The charge integrator detects charges higher than 26.7 $\mu C/cm^2$ and thereby meets the specified requirement.
Finally, the error module combines all the signals from the overvoltage detector, overcurrent detector and the charge integrator. The implemented error module stops further stimulation in case of a detected faulty stimulation and discharges the tissue.
After the improvements proposed in chapter 10, the system is able to meet all the system requirements of (chapter 2). As for the functional requirements, the proposed improved design for DC blockage should be investigated in order to meet the set requirements.

11.2. Recommendations

During this project some interesting topics of research came up. Unfortunately, these could not all be done because of the limited time. Each topic will be introduced briefly for future work.

Charge balancing in the Tissue

Further research can be done in the charge balancing of tissue. Especially if the voltage over the tissue is known, it is possible to accurately balance the charge in the tissue. Several propositions for active charge balancing for this technique have been made [48]. However, with higher frequencies, challenges are introduced and different solutions to charge balancing should be found.

HFCS topology for Biphasic Stimulation

High frequency current switching (HFCS) was discussed in chapter 5 and a concept topology is included in appendix A.1. Currently only a HFCS topology for monophasic stimulation is functional. Additional research into a topology that supports biphasic stimulation while guaranteeing safety for the patient without too much additional overhead could be done.

Practical Failure Analysis of the Neural Stimulator

For the scope of this project it would cost too much time to analyse the failure of the system practically. However it would be good to investigate the working of the system under extreme conditions. It should be researched what happens when one of the components breaks down, and if that could lead to dangerous situations for the patients,

Trigger Level of Detectors

The implementation of the detector sub modules is designed to stop stimulation signals that exceed the safety parameters. The drawback is the delay of a few microseconds in this system. Research could be done to implementations that physically limits the output signal to the safety parameters, thus making it impossible that over stimulation occurs at any time.

Single Fault Safety

In this project, single fault safety was defined as the safe close down of the system. This was done because good documentation on single fault safety of battery powered devices was hard to find. Most of the single fault safety conditions found were only applicable to devices supplied by the mains supply. Further research should be done to single fault safety conditions for battery powered devices.
For the implemented single fault safety switches, the current in case of transistor break down was limited by resistors. However, there was no detection of this breakdown, which means it could remain unnoticed by the user. A solution to this problem should also be researched.

Bibliography

[1] M.C.W. Engelen and P.C. van den Heuvel, "Control & interface module for a high frequency arbitrary waveform neural stimulator," Delft University of Technology, Tech. Rep., 2018.

[2] T. V. A. Salden and S.J.H. Verkleij, "Arbitrary waveform generatorfor for a high frequency arbitrary waveform neural stimulator," Delft University of Technology, Tech. Rep., 2018.

[3] M. B. Chancellor and A. C. Diokno, Eds., *The underactive bladder*. Springer International Publishing, 2016.

[4] B. F.M. Blok, "Sacral neuromodulation for the treatment of urinary bladder dysfunction: mechanism of action and future directions," vol. 1, pp. 85–94, Jan 2018, available at: https://doi.org/10.2217/bem-2017-0003.

[5] J. Groen, J. Pannek, D. C. Diaz, G. D. Popolo, T. Gross, R. Hamid, G. Karsenty, T. M. Kessler, M. Schneider, L. t. Hoen, and B. Blok, "Summary of European Association of Urology (EAU) Guidelines on Neuro-Urology," *European Urology*, vol. 69, no. 2, pp. 324–333, 2016. [Online]. Available: http://www.sciencedirect.com/science/article/pii/S030228381500740X

[6] J. Jamison, S. Maguire, and J. Mccann, "Catheter policies for management of long term voiding problems in adults with neurogenic bladder disorders (review)," vol. 2, p. CD004375, Feb 2004.

[7] R. I. Pettigrew, W. J. Heetderks, C. A. Kelley, G. C. Y. Peng, S. H. Krosnick, L. B. Jakeman, K. D. Egan, and M. Marge, "Epidural spinal stimulation to improve bladder, bowel, and sexual function in individuals with spinal cord injuries: A framework for clinical research," *IEEE Transactions on Biomedical Engineering*, vol. 64, no. 2, pp. 253–262, Feb 2017.

[8] M. J. McGee, C. L. Amundsen, and W. M. Grill, "Electrical stimulation for the treatment of lower urinary tract dysfunction after spinal cord injury," *The journal of spinal cord medicine*, vol. 38, no. 2, pp. 135–146, 2015.

[9] A. Boger, N. Bhadra, and K. J. Gustafson, "Bladder voiding by combined high frequency electrical pudendal nerve block and sacral root stimulation," *Neurourology and urodynamics*, vol. 27, no. 5, pp. 435–439, 2008.

[10] G. E. Ólafsdóttir, "An Implantable Spinal Cord Stimulator with Adaptive Voltage Compliance for Freely Moving Rats," TUdelft, Tech. Rep., 2017.

[11] M. N. van Dongen and W. A. Serdijn, *Design of efficient and safe neural stimulators, A multidisciplinary approach*. Springer, 2015.

[12] N. Bhadra, N. Bhadra, K. Kilgore, and K. J. Gustafson, "High frequency electrical conduction block of the pudendal nerve," *Journal of neural engineering*, vol. 3, no. 2, p. 180, 2006.

[13] H. Schachter, "Vagal nerve blockade for obesity: Vbloc therapy using the maestro rc2 device," *CADTH issues in emerging health technologies*, Sept 2015.

[14] Medtronic, *Test Stimulator 3625 for Deep Brain Stimulation*, Medtronic.

[15] D. R. Merrill, M. Bikson, and J. G. Jefferys, "Electrical stimulation of excitable tissue: design of efficacious and safe protocols," *Journal of Neuroscience Methods*, vol. 141, no. 2, pp. 171 – 198, 2005. [Online]. Available: http://www.sciencedirect.com/science/article/pii/S0165027004003826

[16] B. Piallat, S. Chabardès, A. Devergnas, N. Torres, M. Allain, E. Barrat, and A. L. Benabid, "Monophasic but not biphasic pulses induce brain tissue damage during monopolar high-frequency deep brain stimulation," *Neurosurgery*, vol. 64, no. 1, pp. 156–163, 2009. [Online]. Available: http://dx.doi.org/10.1227/01.NEU.0000336331.88559.CF

[17] A. Scheiner, J. T. Mortimer, and U. Roessmann, "Imbalanced biphasic electrical stimulation: Muscle tissue damage," *Annals of Biomedical Engineering*, vol. 18, no. 4, pp. 407–425, Jul 1990. [Online]. Available: https://doi.org/10.1007/BF02364157

[18] N. d. N. Donaldson and P. E. K. Donaldson, "When are actively balanced biphasic ('lilly') stimulating pulses necessary in a neurological prosthesis? i historical background; pt resting potential;q studies," *Medical and Biological Engineering and Computing*, vol. 24, no. 1, pp. 41–49, Jan 1986. [Online]. Available: https://doi.org/10.1007/BF02441604

[19] Nevro, *Summary of Safety and Effectiveness Data, Senza Spinal Cord Stimulation (SCS) System*, Nevro.

[20] ——, *Physician Implant manual Nevro HF10*, Nevro.

[21] Medtronic, *Dual-program Neurostimulators for Spinal Cord Stimulation (SCS), Synergy Model 7427*, Medtronic.

[22] T. L. Rose and L. S. Robblee, "Electrical stimulation with pt electrodes. viii. electrochemically safe charge injection limits with 0.2 ms pulses (neuronal application)," *IEEE Transactions on Biomedical Engineering*, vol. 37, no. 11, pp. 1118–1120, Nov 1990.

[23] X. Liu, A. Demosthenous, and N. Donaldson, "Five valuable functions of blocking capacitors in stimulators," *Biomed Techn 53 (SUPPL. 1)*, pp. 322–324, 2008.

[24] J.-J. Sit and R. Sarpeshkar, "A low-power blocking-capacitor-free charge-balanced electrode-stimulator chip with less than 6 na dc error for 1-ma fullscale stimulation," *IEEE Transactions on Biomedical Circuits and Systems*, vol. 1, no. 3, pp. 172–183, 2009, pMID: 19109445.

[25] X. Liu, A. Demosthenous, and N. Donaldson, "An integrated implantable stimulator that is fail-safe without off-chip blocking-capacitors," *IEEE Transactions on Biomedical Circuits and Systems*, vol. 2, no. 3, pp. 231–244, Sept 2008.

[26] P. Havel, "How to design safe medical products," 2014. [Online]. Available: http://www.machinedesign.com/medical/how-design-safe-medical-products

[27] A. Connor and E. Ortiz, "Staff solutions for noise reduction in the workplace," *The Permanente Journal*, 2009. [Online]. Available: https://www.ncbi.nlm.nih.gov/pmc/articles/PMC2911833/

[28] *ICL7611, ICL7612 - 1.4MHz, Low Power CMOS Operational Amplifiers*, Intersil.

[29] *INA117P - High Common-Mode Voltage DIFFERENCE AMPLIFIER*, Texas instruments, Dec. 2000.

[30] *LM111-N/LM211-N/LM311-N Voltage Comparator*, Texas instruments, May 1999, rev E.

[31] X. Liu, N. Donaldson, and A. Demosthenous, "An integrated stimulator with dc-isolation and fine current control for implanted nerve tripoles," *IEEE Journal of Solid-State Circuits*, vol. 46, no. 7, pp. 1701–1714, July 2011.

[32] X. Liu, A. Demosthenous, and N. Donaldson, "A dc-isolated fine-controlled neural stimulator," in *2010 Proceedings of ESSCIRC*, Sept 2010, pp. 338–341.

[33] AVX, *T4J – Medical Series HRC4000 Implantable Non Life Support and Non Implantable Life Support, AVX T4JC106K035CRLQ4700*.

[34] ——, *Automotive MLCC - AVX 12103C106K4Z2A*.

[35] A. E. council, "Aec - q200, stress test qualification for passive components," 2010.

[36] *J175 / J176 / MMBFJ175 / MMBFJ176 / MMBFJ177 P-Channel Switch*, On Semiconductor, 2017.

[37] M. Ortmanns, "Charge balancing in functional electrical stimulators: A comparative study," in *2007 IEEE International Symposium on Circuits and Systems*, May 2007, pp. 573–576.

[38] *Medtronic InterStim Therapy model 3889 Lead*, 2002.

[39] *2N7000G Small Signal MOSFET 200 mAmps, 60 Volts*, On Semiconductors, Apr. 2011.

[40] S. Brown and Z. Vranesic, *Fundamentals of Digital Logic with VHDL Design*, 3rd ed. McGraw-hill, 2009, iSBN = 978-007-126880-6.

[41] *CD4071B, CD4072B, CD4075B TYPES datasheet (Rev. D)*, Texas instruments, Aug. 2003, rev D.

[42] I. E. COMMISSION, "Iec 60601-1-11, edition 2.0," *ICS10.040*, 2015.

[43] A. E. council, "Aec - q101, failure mechanism based stress test qualification for discrete semiconductors in automotive applications," 2013.

[44] R. Furtaw, "Texas instruments general quality guidelines," 2017.

[45] "Reliability reports intersil products," www.intersil.com/en/support/qualandreliability.html, last visited: 2018-06-13.

[46] "Reliability reports on semiconductor products," http://www.onsemi.com/PowerSolutions/reliability.do, last visited: 2018-06-13.

[47] M. N. Van Dongen and W. A. Serdijn, "Design of a versatile voltage based output stage for implantable neural stimulators," in *Proceedings - 2010 1st IEEE Latin American Symposium on Circuits and Systems, LASCAS 2010*, 2016, pp. 132–135.

[48] K. Sooksood, T. Stieglitz, and M. Ortmanns, "An active approach for charge balancing in functional electrical stimulation," *IEEE Transactions on Biomedical Circuits and Systems*, vol. 4, no. 3, pp. 162–170, June 2010.

A

Appendices

A.1. Biphasic HFCS

The designed topology for high frequency current switching. This design is based on the monophasic HFCS topology presented in literature [25]. The design made is very conceptually and further research into this design as mentioned in chapter 10 will have to be done. Figure A.1 shows a possible design for biphasic HFCS, the design is quite similar to two monophasic HFCS topologies in parallel with additional switches and adjusted diodes. With this topology it is possible to use biphasic HFCS, however a lot of optimalization needs to be done before this circuit could be effectively implemented.

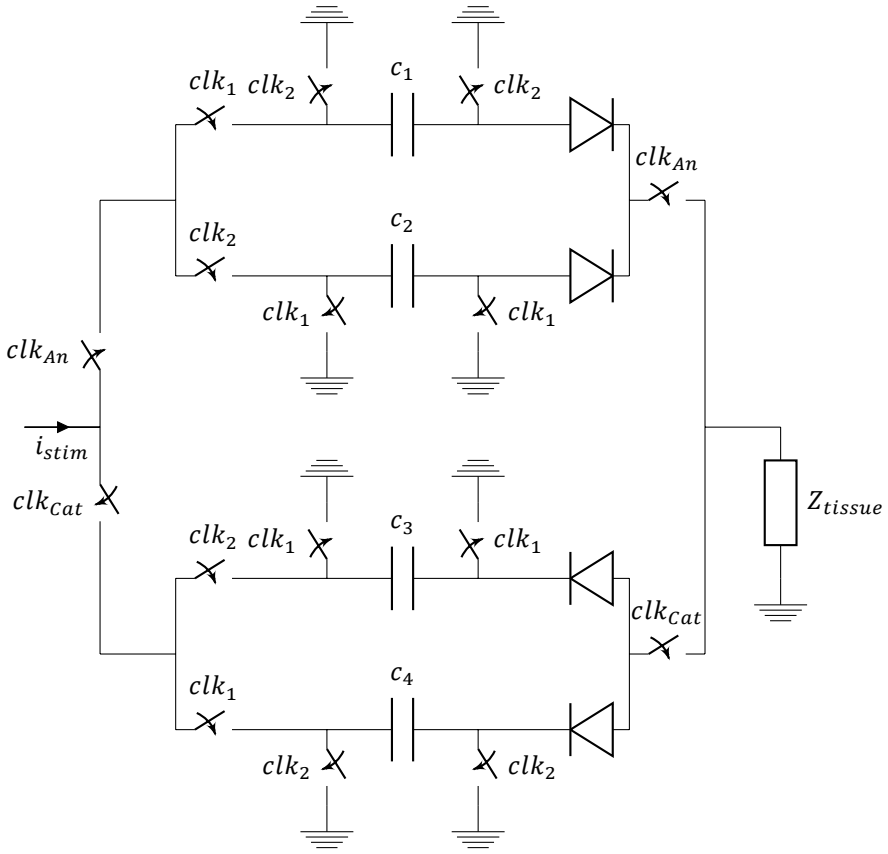

Figure A.1: Biphasic High frequency current switching topology.

A.2. Qualifications of IC's Used

Table A.1: Qualification of semiconductor components used in the safety module.

Manufacturer	Component	Qualification
ON Semiconductors	2N7000 [39]	AEC Qualified
Intersil	ICL7612DCBAZ-T [28]	-
Texas Instruments	INA117P [29]	-
Texas Instruments	LM211P [30]	Model dependent (AEC/military possible)
Texas Instruments	CD4072BE [41]	-
ON Semiconductors	J176 [36]	-